CLM-R269

CLM-R269

UKAEA

Report

APPLICATION OF SOME NOVEL METHODS OF TIME SERIES ANALYSIS TO TOKAMAK DATA

W. ARTER
D. N. EDWARDS

CULHAM LABORATORY
Abingdon, Oxfordshire
1987

C.18

Available from H.M. Stationery Office

Price £5.00

CLM-R269

APPLICATION OF SOME NOVEL METHODS OF TIME SERIES ANALYSIS TO TOKAMAK DATA

W. Arter and D.N. Edwards*

Culham Laboratory, Abingdon, Oxon. OX14 3DB

(Euratom/UKAEA Fusion Association)

Abstract

A time series may be regarded as a structure (manifold) in a multi-dimensional space if delay co-ordinates are used. To such manifolds may be assigned a dimension (not necessarily an integer), a measure of the complexity of the signal, and Lyapunov exponents, which measure the rate at which successive oscillations become decorrelated. In addition a special co-ordinate system, which can help further unravel the complexity of the time series, may be constructed. Successful applications of the first two measures to data from the DITE tokamak are described with an emphasis on issues such as signal-to-noise ratio and minimum sample size. The third technique when applied to DITE data, appears to be useful only as a method for quantifying and removing noise.

*Present address: Rex Thompson & Partners,
Newnhams, West Street, Farnham, Surrey.

August 1986

ISBN 085311 1537

1. Introduction

The main aim of the report is to gain understanding of the signal-to-noise ratio, sampling frequency and sample size required for three novel methods of time series analysis to produce useful results. The importance of these methods is that they provide a quantitative measure of the complexity of the system responsible for the time series. In particular, complicated but nonetheless deterministic behaviour may be distinguished from noise. In addition, the knowledge that a system possesses only a few degrees of freedom should be of great help in modelling such behaviour.

The methods cannot be explained without recourse to a little mathematics. However, the presentation will be mainly heuristic with the number of definitions kept to a minimum. Central to all is the idea of generating a multi-dimensional structure from the data using delay co-ordinates. Suppose we have a time series $X_k = X(t_k)$, $k = 1,\ldots,N$, where N is the total sample size and the t_k are evenly spaced times, Δt apart, then we may construct n-dimensional vectors $\underset{\sim}{x}_k$ by

$$\underset{\sim}{x}_k = \big(X(t_k),\ X(t_k + \tau),\ldots,\ X(t_k + [n-1]\tau)\big), \qquad (1.1)$$

where τ is an arbitrary time interval. It may be shown rigorously that this (delay) co-ordinate system is a good choice provided $[n-1]\tau < P$, a measure of oscillation duration (Takens, 1981). Degeneracy occurs when two components of $\underset{\sim}{x}_k$ are the same, e.g. it is pointless to set $\tau = P$ when the time series has a single period P.

In principle, there is no need to have recourse to this procedure if more than one time series is collected - there is the obvious choice of co-ordinates say (X_k, Y_k, Z_k) if X_k, Y_k, and Z_k are simultaneous samples of the same system but measured at e.g. different places. However these co-ordinates may still be degenerate if it happens that $Y_k \propto Z_k$ for each k; further, there is then a physical restriction on the allowable n.

As a consequence of (1.1) we can conceive of our data as a set of points in an n-dimensional space. We can imagine these joined in order $\underset{\sim}{x}_1, \underset{\sim}{x}_2, \ldots, \underset{\sim}{x}_k, \underset{\sim}{x}_{k+1}, \ldots$ to give an approximation to the trajectory, i.e. the result of joining points $\underset{\sim}{x}_k$ when the sampling is continuous. Clearly in this limit the trajectory is one-dimensional. However for finite sample intervals the points on the trajectory can appear to be space-filling. The first method of analysis assigns a dimension ν to the trajectory. This measure of the signal complexity does not depend on sample interval over a range of Δt and need not be an integer (see Chapter 2).

The second method of analysis gives Lyapunov exponents, which quantify how rapidly nearby trajectories diverge or converge. If the trajectory fills a region of space sufficiently well, it is possible to find a lot of points $\underset{\sim}{x}_\ell$ and $\underset{\sim}{x}_m$ close together but separated by many Δt. By calculating how fast $\underset{\sim}{x}_{\ell+j}$ and $\underset{\sim}{x}_{m+j}$ separate as j increases from 0, and averaging, the Lyapunov exponents associated with the trajectory may be obtained (see Chapter 3).

The third method of analysis seeks a new co-ordinate system for the n-dimensional space that depends on the trajectory. This co-ordinate system has the property that, in the absence of noise, it gives an upper bound $d_M (\leqslant n)$ for the smallest dimension d_s of space in which the trajectory does not intersect itself. d_M therefore provides an upper bound on the number of degrees of freedom of the system responsible for the signal (see Chapter 4).

In summary, Chapter 5 indicates that much of the data routinely collected from DITE tokamak discharges is barely suitable for analysis by all these methods, because the sampling rates are set just too low relative to the characteristic time-scales of in particular the magnetic (Mirnov) oscillations. When sampling rates are increased by a moderate ratio (2.5 to 5), the first method yields dimensions near 2, and the second shows that successive oscillations decorrelate rapidly. The physical significance of these results is then discussed. The signal-to-noise ratio of the data, barely adequate for the first two measures, is too poor for the third. It transpires however that it does

provide a powerful assumption-free method for filtering out noise if the sampling rate is very high (20-50 times normal).

2. Dimensionality Studies

2.1 Introduction

We shall be exclusively concerned with the measure ν first suggested by Young (1982), now associated with the names of Grassberger and Procaccia (1983a,b). Mathematically speaking, ν is a lower bound on the Hausdorff dimension $d_H \geq \nu$: generally it is impractical to calculate d_H directly. Other techniques for estimating d_H have been proposed (Termonia and Alexandrowicz, 1983; Badii and Politi, 1984) and there are other valid definitions of dimensionality (Ott et al, 1984). However, the scheme of Grassberger and Procaccia remains the most popular choice for analysing experimental data (Eckmann and Ruelle, 1985).

Definitions of dimension such as d_H, that need not always give integer values, were motivated by the existence of fractals (Mandelbrot, 1977). These are mathematical objects with a complex self-similar structure: whatever scale we choose to view them on, we can always find a smaller one on which they look the same. The trajectories of many, chaotic dynamical systems turn out to wind through fractals. Using the method of Grassberger and Procaccia we can determine whether an apparently irregular signal is generated by a system of this type and quantify its complexity.

Their definition of ν can be understood in the light of the following (Nicolis and Nicolis, 1984). Consider simple geometrical objects such as the perimeter of an ellipse, a square (with its interior) and a cube, and imagine them sampled at equispaced points. (N.B. a simple sine wave has an elliptical trajectory in delay co-ordinates.) Then, in the case of the ellipse, the number of points of the trajectory within a distance r of a given point upon it is proportional to r^{ν} with $\nu = 1$, provided r is not too large or small, whereas for the square or any other planar object $\nu = 2$ (see Fig. 1), and $\nu = 3$ for the cube. Thus

ν gives the expected dimensions of ordinary objects, yet it does not have to be an integer, as its exact definition (below) makes clear.

First we introduce the correlation integral

$$C(r) = \lim_{N\to\infty} \frac{1}{N^2} \sum_{i\neq j} H(r - |\underset{\sim}{x}_i - \underset{\sim}{x}_j|), \tag{2.1}$$

where H is the Heaviside step function, N is the total number of sample points $\underset{\sim}{x}_i$ that serve to define the geometry of the object, and $|\underset{\sim}{x}_i - \underset{\sim}{x}_j|$ is the distance between two points in n-dimensional space. ν is then defined by

$$\nu = \lim_{r\to 0} \; d \log C / d \log r, \tag{2.2}$$

assuming the limit exists.

The main aim of this section is to determine under what conditions a meaningful value can be assigned to ν. It is immediately evident that the noise associated with any experimental data may affect ν when r is of order of or smaller than the uncertainty in the measurements. Although these matters have received some discussion in the literature (Ben-Mizrachi et al, 1984), the data collected from tokamak experiments is relatively much poorer than has normally been used in the calculation of ν.

The data available from the DITE tokamak is limited by the acquisition unit to a maximum of $N = 4096$ samples per experiment, and has at best 8-bit precision. Typically, signals are sampled every 50 μs, yet the characteristic frequency of the magnetic oscillations is of order 2kHz, giving only 2-3 measures per cycle. Disregarding for the moment the restriction on $n \leqslant 2$ imposed by Takens' theorem (1981), we determine if it is possible to measure ν for an attractor with known properties from data of this quality.

2.2 A Controlled Study of the Lorenz System

We use as control a data-set produced by computing a solution of the Lorenz system (Lorenz, 1963), a third-order set of ordinary differential equations (ODEs) of the form:

$$\dot{a} = \sigma_L(b - a), \quad \dot{b} = -b - ac + r_L a, \quad \dot{c} = ab - \ell_L c. \tag{2.3}$$

for parameters $\sigma_L = 10$, $r_L = 28$, $\ell_L = 8/3$, post-transient solutions are known to lie on a fractal, the Lorenz attractor, with dimension $\simeq 2.05$ (Grassberger and Procaccia, 1983b). $c(t)$ undergoes irregular oscillation with a mean period $P \simeq 0.75$ and amplitude 24. We sample it at intervals $\Delta t = 0.1$, i.e. about 8 measures per cycle, truncating c to the nearest integer. $C'(r) = d \log C / d \log r$ for the resulting record, for which $N = 2000$, is plotted for varying n in Fig. 2a and for small values of τ in Fig. 2b. r is normalised with respect to r_o, where $n^{1/2} r_o$ is the mean absolute deviation of the data about its average value.

Fig. 2a shows the characteristic saturation in the logarithmic slope of $C(r)$ as n is increased greater than ν at a value of 2.1 - 2.2. This agrees with other calculations to about 5%, the expected degree of accuracy (Grassberger and Procaccia, 1983b). At all n we see a change in the slope as r/r_o gets small, due to the noise introduced by the truncation and there is inevitably a saturation as r becomes of order the maximum value of the data. The constant section indicative of a fractal is further shortened as n increases because the delay co-ordinates distort the trajectory more strongly. It is important to verify that ν is independent of the choice of delay co-ordinate, see Fig. 2b. However, as the delay time τ is further increased, $C'(r)$ distorts and increases. When $\tau/\Delta t = 20$, we find $\nu \simeq 3$ (Fig. 2c) and higher τ give even larger ν. This is because we no longer have a good co-ordinate system: the components of each $\underset{\sim}{x}_i$ become decorrelated when $n\tau$ is much greater than P.

We conclude that despite the drastic truncation of the DITE data and the restricted sample size, it is possible to infer the presence of

fractal trajectories. However, the sampling rate is not quite fast enough relative to the oscillation frequency: the restriction on $n\tau$ makes it difficult to check reliably that ν is independent of n and τ.

2.3 A Controlled Study of Random Data

If for some reason we cannot estimate ν very well, we would still like to be able to distinguish whether a signal has a deterministic component. Thus, we have undertaken a study of ν for data-sets generated using the NAG routine GØ5DAF to produce random values on $(-1,1)$. A totally random signal is expected to give $\nu \simeq n$ for all n, because its constituent points should scatter evenly throughout a space of any dimension. Nevertheless we expect, for a finite sample size, some clustering as n increases, and we seek to determine this.

τ is irrelevant in this case. Fig. 3a shows a typical plot of $C'(r)$ as n increases. Fig. 3b shows how for a sample size $N = 2000$, ν becomes significantly less than n as n increases beyond 8. Clearly we cannot expect to calculate ν of this magnitude with only a few thousand measurements. We remark that only $\sqrt[8]{2000} \simeq 2.5$ points lie along each side of an 8-dimensional object using this sample size. However, if we demand a minimum of 10 points per side, $N \geqslant 10^8$, which may be an unduly pessimistic estimate of the amount of data required.

2.4 First application to DITE Data

As Section 2.2 makes clear, much of the magnetic data routinely collected from the DITE tokamak is inadequate for good dimensionality studies. A few records are available with $\Delta t = 25\,\mu s$, and from these we select discharge 24591 for study (Arter and Edwards, 1985). For this shot, the standard diagnostics indicate a total plasma current $I = 125kA$, toroidal magnetic field, $B_\phi = 2T$ ($q_L = 4.6$), and a line-averaged density $\bar{n}_e = 1.6 \times 10^{19} m^{-3}$.

The DITE data is provided by 8 Mirnov coils, distributed uniformly in poloidal angle around the tokamak inside the vacuum vessel in one vertical

plane, see Fig. 4a. The local $\dot{B}_\theta$, the time rate of change of the poloidal field, is sampled by each coil simultaneously.

The 4096 data points cover approximately the first 100 ms of discharge 24591. We discard the first 43 ms of data, which corresponds to the plasma current rise time; the current plateau phase ("flat top") of the discharge might be expected to form a simpler system than the transient phase, the properties of which might also depend more strongly on discharge number.

We consider the time signal from coil 1, now represented by a record with $N = 1920$, duplicating the analysis of the Lorenz attractor. Figs. 5a and 5b show that the resulting correlation functions have the same qualitative behaviour as Lorenz, and a similar slope (at least for larger r). Since the number of points in the sample is small, it is adequate to estimate gradients and their errors graphically, giving $\nu = 2.1 \pm 0.3$. $C(r)$ at smaller r has a steeper logarithmic slope close to n, i.e. this level of signal is uncorrelated for $n \leqslant 6$ and might well be identified with experimental noise (Ben-Mizrachi et al, 1984), but see the discussion in Chapter 5.

Taking $n = 4$ and $\tau = 6\Delta t$ ($=150\,\mu s$) we find that coils 3, 4 and 7 give slopes consistent with the above estimate for ν suggesting that we are measuring a global feature of the discharge. As a check, we use the signals at a given instant from coils 1, 2, 3 and 4 to construct a 4-dimensional vector and find $\nu \simeq 2.2$ using 1920 vectors of this type, see Fig. 5c.

Further analysis of the signal supports the contention that an attracting fractal trajectory ("strange attractor") underlies the magnetic behaviour of discharge 24591 (Arter and Edwards, 1985, 1986). The sample size however is apparently insufficient to confirm the convergence of ν with respect to increasing N (Fig. 5d). Since this is ultimately the only means of demonstrating the presence of a fractal and that ν has been accurately calculated, the strange attractor interpretation is not completely unambiguous.

2.5 Other DITE Discharges

While the ohmically heated density limit on DITE was being investigated in late 1985 we were able to obtain data sampled with $\Delta t < 25\mu s$. In this section, we consider the flat-top phase of another discharge, number 27649 and data collected prior to disruption on discharges 27792 and 28030. The sampling intervals Δt were $5\mu s$, $2\mu s$ and $10\mu s$ respectively. For all four shots, I = 150kA and $B_\phi = 2T$. Data prior to disruption from an earlier discharge 26246 was found to have $\Delta t = 10\mu s$ and is analysed. Further description of all these data-sets is provided by Table I.

Discharge 27649 has $\bar{n}_e$ increasing from $2.3 \times 10^{19} m^{-3}$ at t = 100 ms to $8.1 \times 10^{19} m^{-3}$ at t = 500 ms. During the discharge, a soft X-ray (SXR) signal from a chord located as shown in Fig. 4b, outside the sawtooth inversion radius was available in addition to magnetic data from coil 7, positioned as in Fig. 4a. The two signals were each recorded starting at a time 275.64 ms into the discharge, and N = 3894.

Plotting $C'(r)$ for the soft X-ray signal suggests it has at least two components, one of logarithmic slope $\simeq 1.2$ at large r and another with slope $\simeq 3.2$ at smaller r (Fig. 6a). Taking N = 1944 supports this interpretation and the ν values found. There is little evidence that noise is affecting the data. The $\nu \simeq 1$ component is easily interpreted as corresponding to the characteristic sawtooth oscillation.

Fig. 6b shows $C'(r)$ for the Mirnov data, which shows no evidence for any saturation. This is rather curious, because it would otherwise be natural to interpret the high ν component of the soft X-rays as due to superimposed Mirnov oscillations. $\nu \simeq 3$ is a typical value for Mirnov data collected on TOSCA and JET (Coté et al, 1985). One possible explanation is that the $\nu \simeq 3.2$ component of the DITE soft X-rays is in some way spurious.

The data for discharge 28030 consists again of a soft X-ray signal from even further outside the inversion radius than shown in Fig. 4b,

together with magnetic signals collected from coil 8. Sampling was from times 480.01 - 507 ms (N = 2700) into the discharge, which disrupted (i.e. had a loop voltage spike) at $t = 511$ ms when $\bar{n}_e = 3.3 \times 10^{19} m^{-3}$. $C'(r)$ for the 2 signals is plotted in Fig. 7. The soft X-rays are shown to have two components with $\nu \simeq 1$ and $\nu \simeq 1.9$ respectively, similar to discharge 27649. This time the Mirnov data yield $\nu \simeq 1.8 \pm 0.1$, and so account for the high ν part of the soft X-ray signal.

For discharge 26246 Mirnov data from 8 coils is available, but no soft X-ray information. Sampling was from times 170 - 198 ms into the discharge when $\bar{n}_e = 3.6 \times 10^{19} m^{-3}$: there was a soft disruption at $t =$ 190 ms, preceded by a factor 4 decrease in Mirnov frequency starting at t = 188 ms. The data was therefore divided into two parts, the first "A" with $N = 1800$ covering $t = 170 - 188$ ms, and "B" with $N = 1000$ for the remaining times to 198 ms. Part A from coils 1, 2 and 6 gave three values of $\nu \simeq 1.7 \pm 0.1$. The signals in part A at a given instant from coils 1, 2, 3 and 4 and from coils 5, 6, 7 and 8 were used to construct vectors with $n = 4$ and both gave $\nu \simeq 1.6$. It seems that $\nu \simeq 1.6$ corresponds to a global feature of the discharge. Analysis of the part B samples gave ambiguous results - the results are consistent with a ν of anything between 1.5 and 2.5.

Lastly we considered data collected from coils 5 and 7 of discharge 27792, spanning times $t = 455.101 - 459.191$. The loop volts and soft X-rays indicate that there was a soft disruption at $t = 457.1$, followed by a hard one at 459.5 ($\bar{n}_e = 6.7 \times 10^{19} m^{-3}$). Inspection of the $C'(r)$ plot in Fig. 8a yields a slope of 1.2 for coil 5. The signal from coil 7 is much harder to interpret since there are no prominent straight line sections in Fig. 8b, but there is some evidence for $\nu \simeq 1$. These ν-values presumably relate to the 10 cycles or so of the gross oscillation. From Fig. 8, the data appears to be such that a lower amplitude component with $\nu > 2$ would not be detectable.

3. Lyapunov Exponents

3.1 Basic Concepts

The concept of Lyapunov exponent derives from linear stability studies of steady solutions to ordinary differential equations (ODEs).

Small amplitude perturbations $\propto e^{\lambda t}$ are superimposed and for an nth order system, λ is found to satisfy an nth order polynomial. Generically, there are n distinct roots λ_i, $i = 1,.., n$, each associated with a particular perturbation eigenvector $\underset{\sim}{e}_i$, $i = 1,..., n$. The λ_i, arranged in descending order, constitute the spectrum of Lyapunov exponents for the fixed point. However, this is just one instance of their use: the definition of Lyapunov exponents is framed much more generally, so that they may be assigned to time dependent solutions of ODEs. Loosely speaking, the λ_i at each point on the trajectory are calculated and averaged over.

More precisely, let us introduce the n-dimensional system of ODEs with trajectory $\underset{\sim}{x}(t)$,

$$\dot{\underset{\sim}{x}} = \underset{\sim}{F}(\underset{\sim}{x}). \tag{3.1}$$

At a point on the trajectory, say $\underset{\sim}{x}(0)$, we may define tangent vectors $\underset{\sim}{e}_i(0)$ analogously to the $\underset{\sim}{e}_i$ above. As t increases and the trajectory is traversed the $\underset{\sim}{e}_i$ change continuously in both magnitude and direction. We may write

$$\underset{\sim}{e}_i(t) = \underset{\approx}{A}(t).\underset{\sim}{e}_i(0). \tag{3.2}$$

In the light of the first paragraph it is reasonable to assume that the length of each $\underset{\sim}{e}_i$ (while it remains small) varies exponentially as the trajectory is traversed. Hence we define

$$\lambda_i = \lim_{t\to\infty} \frac{1}{t} \ln \frac{\left|\underset{\sim}{e}_i(t)\right|}{\left|\underset{\sim}{e}_i(0)\right|}, \tag{3.3}$$

from now on neglecting the directional changes in the $\underset{\sim}{e}_i$.

The definition (3.3) is not immediately suitable for numerical calculation since any exponential variation in $\left|\underset{\sim}{e}_i(t)\right|$ will rapidly

generate very large or small numbers, hence it is necessary to renormalise $\underset{\sim}{e}_i$ from time to time so that $\left|\underset{\sim}{e}_i(t)\right| = 1$. Further, when we have a trajectory $\underset{\sim}{x}(t_j)$ defined by a discrete set of data, there is more than one way to calculate λ_i.

3.2 Description of the Methods

We consider two methods: the first "SS" method was proposed by Sano and Sawada (1985) and Eckmann and Ruelle (1985). Conceiving the trajectory as a line in n-dimensional space, select a point $\underset{\sim}{x}_j$ on the line, and seek near neighbours $\underset{\sim}{x}_{k_i}$ of $\underset{\sim}{x}_j$. "Near" means the points $\underset{\sim}{x}_{k_i}$ lie such that $\left|\underset{\sim}{x}_{k_i} - \underset{\sim}{x}_j\right| \leqslant \varepsilon$, where ε is chosen so that there are almost always at least $M > 1$ near neighbours. In the time interval $\theta = p\Delta t$, $\underset{\sim}{x}_j$ evolves to $\underset{\sim}{x}_{j+p}$ and $\underset{\sim}{x}_{k_i}$ to $\underset{\sim}{x}_{k_i+p}$. Introducing $\underset{\sim}{Y}_i = \underset{\sim}{x}_{k_i} - \underset{\sim}{x}_j$ and $\underset{\sim}{Z}_i = \underset{\sim}{x}_{k_i+p} - \underset{\sim}{x}_{j+p}$, we can write

$$\underset{\sim}{Z}_i = \underset{\approx}{A}(j)\underset{\sim}{Y}_i, \quad i = 1,\ldots,M , \tag{3.4}$$

where $\underset{\approx}{A}(j)$ indicates an estimate for $\underset{\approx}{A}(t)$ (3.2) at the time t when $\underset{\sim}{x}(t) = \underset{\sim}{x}_j$. $\underset{\approx}{A}(j)$ is optimally estimated by least squares fitting (Sano and Sawada, 1985) and can then be used to estimate λ_i as

$$\lambda_i = \lim_{K\to\infty} \frac{1}{K\theta} \sum_{j=1}^{K} \ln \left|\underset{\approx}{A}(j).\ \underset{\sim}{e}_i(j-1)\right| . \tag{3.5}$$

$\underset{\sim}{e}_i(0)$ may be any orthonormal set of n-dimensional vectors: the $e_i(j)$ are calculated from $\underset{\approx}{A}(j).\underset{\sim}{e}_i(j-1)$ using the standard Gram-Schmidt orthnormalisation procedure. After a few iterations the $\underset{\sim}{e}_i(j)$ become a good approximation to the $\underset{\sim}{e}_i(t_j)$, ordered corresponding to λ_i decreasing.

The second, "WSSV" method, due to Wolf et al (1985) does not claim to be able to calculate negative exponents, although it has much in common with the first. Further, we have implemented only the version that calculates the largest exponent. This is done by choosing a single near

neighbour $\underset{\sim}{x}_{k_1}$ to the point $\underset{\sim}{x}_{j_1}$, and calculating lengths L_{j_1+p} defined by

$$L_{j_1+p} = \left|\underset{\sim}{x}_{j_1+p} - \underset{\sim}{x}_{k_1+p}\right|. \tag{3.6}$$

Eventually L_{j_1+p}/L_{j_1} becomes too large at some $p=p_1$ as the trajectories sampled by $\underset{\sim}{x}_{k_1+p}$, $\underset{\sim}{x}_{j_1+p}$ diverge. We replace $\underset{\sim}{x}_{k_1+p_1}$ by some $\underset{\sim}{x}_{k_2}$ close to $\underset{\sim}{x}_{j_2}$ where $j_2=j_1+p_1$ and repeat. It follows that we can estimate

$$\lambda_1 = \frac{1}{T} \sum_{i=1}^{K} \ln (L_{j_{i+1}}/L_{j_i}), \tag{3.7}$$

where T is the time taken to get from $\underset{\sim}{x}_{j_1}$ to $\underset{\sim}{x}_{j_K}$.

For both methods we plot a running average of λ_i against increasing number of iterations to give an indication as to whether convergence has occurred. The SS method is claimed to be superior to the WSSV one, because it tracks an arbitrary vector, whereas the latter is more tied to the data-points. However, our experience indicates the SS method is much less robust.

3.3 The SS Method Applied to the Lorenz System

As in Section 2, we set up a data-set to act as control using the Lorenz system, Eqn.(2.3). To compare directly with Sano and Sawada (1985), we took $\sigma_L = 16$, $r_L = 40$ and $\ell_L = 4$. The resulting c(t) has a characteristic time-scale of 0.5 and a mean amplitude of 16. c(t) was sampled at $\Delta t = 0.035$ and the values were rounded to the nearest one-eighth to give a data-set with a signal-to-noise ratio as low as the best DITE data.

Table II shows the effect of varying the parameters ε, τ, θ and M. M is the maximum number of vectors used in forming (3.4): increasing the number of vectors used in (3.4) improves the accuracy of the calculation. Keeping M low, however, saves computer time, since otherwise the whole data-set will be searched for near neighbours of each

point, giving a N^2 operation count. Taking $M=n=3$ gives a very poor result (Table II, Run 1) and although $M=6$ gives as good a result as $M=15$ (suggesting that there are on average no more than 6 near neighbours of each point), it is apparent that the λ_i determinations are so poor that accuracy considerations must outweigh those of cost, and so $M \geqslant 6$ for the remaining calculations, as suggested by Sano and Sawada (1985). ε, measured in units of max(c)-min(c), is the nearness parameter. Reducing ε to 0.015 (Run 5) has a similar effect to taking M small, implying there are on average too few near neighbours at this ε. Increasing ε to the maximum suggested by Sano and Sawada (1985) improves the λ_i estimates, particularly when $M=15$.

Runs 8-20 show that the poor estimate $\lambda_i=(2, -0.8, -16)$ compared to the known values of $\lambda_i=(1.37, 0, -22.37)$ is not simply due to a particular choice of τ and θ. The computed results are independent of the lag-time τ in the range $\Delta t \leqslant \tau \leqslant 5\Delta t$, but it is clear that taking $\theta > 2\Delta t$ badly affects the λ_3 estimate. The reason for the 50% errors in λ_1 and λ_3 seems to lie partly in our choice of the c-variable to reconstruct the Lorenz trajectory. Table IIb shows that using the a-variable to generate a data-set with otherwise the same properties as that studied in Table IIa gives a much better estimate for the λ_i provided $\theta \leqslant 2\Delta t$, $\tau \leqslant 5\Delta t$. However, both sets of results in Table II show that the apparent convergence of an iteration (inevitably a rather subjective criterion) is no indication with data of this quality of the accuracy of the λ_i calculated, and so we do not consider it further.

c is not a generic variable of the Lorenz system since its oscillations do not reverse unlike those of a and b, and this may explain the large error, since parts of the trajectory that are otherwise well separated are folded together when c(t) is used in reconstructions. Nevertheless the lack of robustness demonstrated by the method is worrying for application to experimental data. There is another difficulty concerning the choice of n in such cases. $n=3$ is known for the Lorenz system, but for systems with an unknown number n_λ of Lyapunov exponents, taking $n > n_\lambda$ leads to spurious exponents being found (J.A. Vastano and E. Kostelich, private communication). Although n_λ can be estimated by study of the eigenvalues of $\underset{\approx}{A}$, Eqn.(3.4), if

the data is very clean (Sano and Sawada, private communication), our data is too noisy for this to work. For the sample of Table IIb, taking $n=4$, we discover that the eigenvalue of $\underset{\approx}{A}$ corresponding to the spurious λ_i is the same size as that corresponding to $\lambda_i = -21.37$. For the experimental data, we shall have to assume that the appropriate n is given by $\max([\nu],3)$, where $[\nu]$ denotes the first integer larger than ν.

3.4 Application of the SS Method to Experimental Data

If we re-express the requirements $\tau \leqslant 5\Delta t$, $\theta \leqslant 2\Delta t$ for the SS method in terms of the characteristic time of the system (see Table I), it appears that only the magnetic signals from discharges 28030 and 24591 are sufficiently well sampled. Even so, we are very restricted as to the allowable τ and θ, with 28030 giving the best data-set for our purposes.

Parts (a)-(c) of Table III show that λ_i for discharge 28030 still depend quite strongly on τ, θ and n. Since the signal is by inspection aperiodic, we have to take $n \geqslant 3$ and $\nu \simeq 1.8$ suggests we should take $n = 3$. Table IIIa further indicates we should attach less weight to λ_i from the larger values of τ/θ. Discarding $(\tau,\theta)/\Delta t = (2,1), (3,1), (3,2)$ and averaging the remaining 3 points gives $\lambda_i = (33, 0.2, -49)$. The only conclusion that may be safely drawn from Table IIIb is the λ_i spectrum has shape $(+, 0, -)$, similar to the Lorenz system. Nevertheless we go on to use it to estimate an upper bound d_λ for d_M. The formula for any d_λ is given in Eckmann and Ruelle (1985), after Frederickson et al (1983). For the averaged λ_i we find $d_\lambda \simeq 2.7$, which seems very high but not unreasonably so, since $d_\lambda \propto 1/\lambda_3$ and $|\lambda_3|$ may be systematically under-estimated as in Table IIIa.

For discharge 24591, where $\nu \simeq 2.1$ suggests we should take $n=3$, Table IIId and IIIe again indicate that the λ_i spectrum is of form $(+, 0, -)$. The scatter with τ and θ is so high that it is again difficult to assign more precise values to the λ_i. Taking coils 1(IIIc) and 4(IIId) together and neglecting λ_i for $(\tau,\theta)/\Delta t = (2, 1)$ gives an average $\lambda_i = (14, -0.1, -18)$. It follows that $d_\lambda \simeq 2.8$ (assuming $\lambda_2 = 0$), which is high, presumably for the same reasons as before. It is

apparent that we cannot put too much faith in the smaller λ_i found by the SS procedure.

3.5 The WSSV Method

As before, we set up a control data-set using the c-variable of the Lorenz system. For comparison with Wolf et al (1985) we take $r_L = 45.92$ ($\sigma_L = 16$, $\ell_L = 4$), but unlike in the previous work we do need not to discretise the sample since their method demands that we do not calculate L_{j_1} (see Eqn.(3.6), p=0), L_{j_2}, L_{j_3}, etc. for points separated by less than a distance ε_{in}. Taking the suggested value for $\varepsilon_{in} = 0(10^{-2})$ has roughly the same effect as rounding the sample to the nearest one-eighth (c.f. Section 3.3). We use a smaller total sample than for the SS method, N = 1998.

Table IV lists the values of λ_1 found by the WSSV method. From these we conclude that it is very much more robust than the SS method with respect to τ, θ and ε variations, although taking $n \geq 4$ does degrade the results significantly. There is a noticeable trend towards lower λ_1 as $\theta/\Delta t$ increases beyond 6, while picking $\tau/\theta \geq 2$ can give very misleading results, just as for the SS method. A notable difference is that this data-set has a $P/\Delta t$ (a characteristic dimensionless time-scale) of 4.5, compared to $P/\Delta t = 14$ in the case of Table II. Thus all of the magnetic data may be meaningfully examined using the WSSV technique, assuming the critical ratios are θ/P and τ/P.

Tables V, VI and VII list λ_1 for discharges 24591, 26246 and 28030 respectively. In each, a trend towards decreasing λ_1 with increasing $\theta/\Delta t$ is evident and high τ/θ gives discrepant λ_1. These trends are very much more pronounced than with the test data-set. Making allowance for them, we see that $\lambda_1 \simeq 8$ for discharge 24591, $\lambda_1 \simeq 25$ for 26246 and $\lambda_1 \simeq 35$ for 28030. Where comparison with SS can be made, these λ_1 lie within the scatter (Table III), which is encouraging.

To compare the various systems we normalise their exponents with respect to characteristic frequencies. The Lorenz system has a $\lambda_1 P$ of 0.7 at $r_L = 40$ and 1.0 at $r_L = 45.92$. These values are comparable with

a $\lambda_1 P$ of 0.8 for DITE discharge 24591. The other discharges have $\lambda_1 P \simeq 3$. Naturally the key point is that λ_1 is positive, implying that nearby trajectories diverge exponentially and supporting the strange attractor interpretation. Further, the larger the trajectory divergence, the smaller should be the maximum useful delay time, hence it is not too surprising that λ_1 for discharges 26246 and 28030 depend sensitively on τ. However, the λ_1 estimate for 24591 also shows a strong τ-dependence - see further discussion in Chapter 5.

3.6 Kolmogorov Entropy Estimation

Strictly speaking, this section should be part of Chapter 2, but its results relate to the Lyapunov spectrum. For our purposes it is not necessary to define the Kolmogorov entropy K. We shall be concerned with the related K_2 entropy which satisfies $K_2 \leqslant K$ (Grassberger and Procaccia, 1983c). Since it is rigorously true that $K \leqslant \sum_i (\lambda_i > 0)$, with equality in many cases (Eckmann and Ruelle, 1985), K_2 also provides a lower bound for the sum of the positive Lyapunov exponents. A working definition of K_2 is

$$K_2 = \lim_{\substack{n \to \infty \\ r \to 0}} \frac{\ln C_n(r) - \ln C_{n+1}(r)}{\tau} , \qquad (3.8)$$

where the suffix n on the correlation function (see (2.1)) denotes that it is calculated in an n-dimensional space, and the normalisation of r is independent of n.

Our principal difficulty is that n of up to about 20 are required for a reliable estimate of K_2 (Grassberger and Procaccia, 1983c), yet it should be evident from Chapter 2 that $C_n(r)$ for DITE data is badly distorted when $n \geqslant 6$, essentially because of the poor statistics. However, it provides a further cross-check on the poorly determined values of λ_i. Some indication of the reliability of the results obtained is given by comparing estimates of K_2 at different n.

No sensible estimate for K_2 is yielded by discharge 24591. For discharge 26246, coil 2, two sets of estimates were obtained at points

$\log_{10}(n^{1/2}r/r_o) = 0$ and 0.2, the first being 9.3, 9.4, 8.3 and 8.1 ms^{-1} and the second 6.4, 6.6, 6.2 and 5.8 ms^{-1} ($n = 3 - 6$ in each case). This is to be compared with $\lambda_1 = 25\ ms^{-1}$ from Section 3.5. The K_2 estimates grow steadily as r diminishes to values where $C_n'(r)$ always increases with n, and thus their interpretation is not clear. Repeating the analysis for the magnetic signal from discharge 28030 yields $K_2 \simeq 14\ ms^{-1}$ ($\log_{10}(n^{1/2}r/r_o) = 0.2$) against a $\lambda_1 = 35\ ms^{-1}$.

Although no values for λ_i, K_2 or K have been published for the Lorenz data considered in Chapter 2, we can still check that the K_2 estimates decrease above zero with increasing n as theory predicts. It transpires that the estimates behave correctly only for $\log_{10}(n^{1/2}r/r_o) \leq -1$. Moreover it is theoretically impossible that $\lambda_1 > K_2$. It seems we must attach a very low level of significance to the K_2 values found above. Nevertheless the indications that $K_2 > 0$ are of value in that they provide further evidence that the systems studied are chaotic.

4. Phase-space Reconstruction

We shall be principally concerned with the method of Broomhead and King (1986). Before considering their technique, we illustrate what can be gained by reconstructing a trajectory using a delay co-ordinate system (which can be used even when the newer technique fails). Fig. 9 exhibits the magnetic signal from discharge 28030 using delay co-ordinates. There is evidence for some coherent structure even in two dimensions (Fig. 9a) and Fig. 9b, a 3-D stereo plot makes this more apparent. This is consistent with the derived exponent $\nu \simeq 1.8$ for the discharge, whereas the large ν signal from discharge 27649 appears completely structureless even in 3-D.

We remark that the portrait of an attractor in delay co-ordinates depends strongly on the choice of delay time τ. There is no quantitative and little qualitative information to be gained from plots such as Fig. 9, which essentially serves only to support the case for low

ν for discharge 28030 made in Chapter 2. The Broomhead-King method removes the arbitrariness in the choice of co-ordinates.

4.1 Description of the Method

The technique described here was proposed by Broomhead and King (1986). The idea is to find the co-ordinate system of smallest dimension d_s with respect to which a trajectory does not intersect itself. However, it turns out that we can only find a bound d_M for d_s such that $(d_M - 1)/2 \leqslant d_s \leqslant d_M$.

Rigorous theory based on the calculus of manifolds proves the above result for d_M which is referred to as the embedding dimension. Why this is the state of affairs can be partly understood from consideration of the perimeter of a circle. Clearly this constitutes a one-dimensional object, since it is only a line segment bent upon itself. However, unlike the line segment, the topology of the circle is such that we cannot describe it in a Cartesian co-ordinate system R^k of dimension k less than two (and there are one-dimensional shapes which, consistent with the above bound, can only be realised in R^3). Nonetheless, frequently $d_s = d_M$.

The Broomhead and King reconstruction (1986) always takes place in a Cartesian co-ordinate system. It entails forming the trajectory matrix $\underset{\approx}{T}$,

$$\underset{\approx}{T} = N_1^{-1/2}(\underset{\sim}{x}_1, \underset{\sim}{x}_2, \ldots, \underset{\sim}{x}_{N_1}), \tag{4.1}$$

where N_1 is an integer just less than N if we use delay co-ordinates. The orthonormal basis required $\underset{\sim}{o}_i, i=1,..,n$, is obtained by diagonalising $\underset{\approx}{V}=\underset{\approx}{T}.\ \underset{\approx}{T}^T$ (where suffix superscript T denotes matrix transpose), i.e. it satisfies

$$\underset{\approx}{T}.\ \underset{\approx}{T}^T.\ \underset{\sim}{o}_i^T = s_i\ \underset{\sim}{o}_i^T\ ,\ i = 1,\ldots,n, \tag{4.2}$$

where the s_i are real since $\underset{\approx}{V}$ is symmetric.

To explain why we choose $\underset{\sim}{o}_i$ in this way, we need some results from

linear algebra. First, note that arbitrary vectors in the d_M-dimensional vector space spanned by the $\underset{\sim}{x}_i$ ($d_M \leq n$) can be generated by multiplying (4.1) by N_1-dimensional vectors. In particular, $\underset{\sim}{a}_i \in R^{N_1}$ may be found so that

$$\underset{\approx}{T}\cdot \underset{\sim}{a}_i = \sigma_i \underset{\sim}{c}_i^T, \quad i = 1,\ldots,d_M, \tag{4.3}$$

where the σ_i are so far arbitrary and the $\underset{\sim}{c}_i$ are orthonormal vectors. If $d_M < n$, by standard results there exist vectors $\underset{\sim}{c}_i$, $i = d_M + 1,\ldots,n$, to complete the basis and there must also be corresponding and distinct vectors $\underset{\sim}{a}_i$ such that $\underset{\approx}{T}\cdot \underset{\sim}{a}_i = 0$, $i = d_M + 1,\ldots,n$. The additional $\underset{\sim}{c}_i$ therefore correspond to $\sigma_i = 0$.

We will now show that for an appropriate choice of σ_i, $\underset{\sim}{c}_i = \underset{\sim}{o}_i$. Multiply (4.3) by its transpose to give

$$\underset{\sim}{a}_j^T \cdot \underset{\approx}{T}^T \underset{\approx}{T}\cdot \underset{\sim}{a}_i = \sigma_i \sigma_j \delta_{ij}, \quad i, j = 1,\ldots,n, \tag{4.4}$$

where δ_{ij} is the Kronecker delta, but the summation convention is not employed. The $N_1 \times N_1$ matrix $\underset{\approx}{U} = \underset{\approx}{T}^T\cdot \underset{\approx}{T}$ is real symmetric and therefore has orthonormal eigenvectors $\underset{\sim}{b}_i$, $i = 1,..,N_1$, forming a basis for R^{N_1}. Since

$$\underset{\approx}{U}\cdot \underset{\sim}{b}_i = \underset{\approx}{T}^T\cdot \underset{\approx}{T}\cdot \underset{\sim}{b}_i = \mu_i \underset{\sim}{b}_i, \quad i = 1,..,N_1, \tag{4.5}$$

the $\underset{\sim}{b}_i$ satisfy (4.4) if $\sigma_i^2 = \mu_i$, $i = j \leq n$, i.e. we may identify $\underset{\sim}{a}_i$ and $\underset{\sim}{b}_i$ for $i \leq n$. If now (4.3) is multiplied by $\underset{\approx}{T}^T$, the left-hand-side may be simplified using (4.5), when a further multiplication by $\underset{\approx}{T}$ gives

$$\mu_i \underset{\approx}{T}\cdot \underset{\sim}{a}_i = \sigma_i \underset{\approx}{T}\cdot \underset{\approx}{T}^T\cdot \underset{\sim}{c}_i^T, \quad i = 1,\ldots,n. \tag{4.6}$$

Hence, using (4.3), we have

$$\sigma_i(\underset{\approx}{T}\cdot\ \underset{\approx}{T}^T\cdot\ \underset{\sim i}{c}^T - \mu_i\ \underset{\sim i}{c}^T) = 0,\ i = 1,\ldots,n. \tag{4.7}$$

Thus we only need choose $\mu_i (= \sigma_i^2) = s_i$ to ensure $\underset{\sim i}{o} = \underset{\sim i}{c}$, each i.

From these results, the first d_M of the $\underset{\sim i}{o}$ span the space in which the $\underset{\sim i}{x}$ lie and from (4.2) $|\sigma_i|$ measures $|\underset{\approx}{T}\cdot\underset{\sim i}{o}|$, the projection of the trajectory matrix on $\underset{\sim i}{o}$. The trajectory may therefore be reconstructed as

$$\underset{\approx}{T}^r = \sum_{i=1}^{d_M} \underset{\sim i}{o}\cdot(\underset{\sim i}{o}^T\cdot\ \underset{\approx}{T}). \tag{4.8}$$

The set of values σ_i^2 arranged in descending order is known as the singular spectrum. In practice, all $\sigma_i^2 \neq 0$ due to the presence of noise. However, white noise is easily discriminated because it increases each σ_i^2 by a constant amount. Thus spurious components may be rejected by finding the point at which the singular spectrum flattens (Broomhead and King, 1986).

The distinction between the method of this section and those in Sections 2 and 3 is that it probes only the smallest scales of a trajectory. A little thought convinces one that if the components of the $\underset{\sim i}{x}$ (delay co-ordinates assumed) are so spaced as to sample the large-scale structure of a trajectory then the $\underset{\sim i}{x}$ can fill a space of arbitrary dimension n. The lag time has to be so small that vectors $\underset{\sim i}{x}$ can be constructed that are not affected by the global changes in the trajectory (and so it is not necessary that n be as restricted as in Chapters 2 and 3). The difficulty is then that all the components of each vector are nearly the same. $\underset{\sim 1}{c}$ is thus always approximately $(1,1,..,1)$, and an order of magnitude more power (as measured by σ_1^2) is assigned to the first projection $\underset{\approx}{T}\cdot\underset{\sim 1}{c}$ than to the second. Components (projections) which are required to ensure the trajectory is non-intersecting may therefore easily either be lost in the noise or badly contaminated by it.

4.2 Application to Test Problems

We illustrate the method using a data-set constructed by sampling the function $f_e(t) = \exp(3[t - 1/2])\sin(60\pi t)$ on the interval $0 \leqslant t \leqslant 1$ at 3000 equally spaced times. There are 30 oscillations in the data, hence 100 points sample each period. The exponential ensures the amplitude varies by a factor 20, from 0.16 to 3.2 in the root-mean-square. In delay co-ordinates f_e maps out a spiral, $d_s = 2$, and we should expect this to be the embedding dimension.

Fig. 10a plots the singular spectrum for the spiral showing indeed that only two of the σ_i^2 are significantly different from zero and Fig. 10b shows the resulting reconstruction. The other components of the signal, apart from the first two, $\underset{\approx}{T}\cdot\underset{\sim}{c}_i$, $i = 3,\ldots,n$, consist of noise at the level of the precision of f_e (24-bit).

Now we add to each data-point in the sample of f_e a random number sampled from a Gaussian distribution with zero mean and a root-mean-square (r.m.s.) of 0.25. The singular spectrum from Fig. 10c still indicates only two components, but now the noise floor has risen to be only 0.5 in the logarithm below the smaller "real" component. It is evident that significant components of the signal could be lost in the noise. The phase space reconstruction in two dimensions (Fig. 10d) shows many (spurious) intersections, thus it incorrectly suggests $d_s > 2$. Only when the noise level is reduced to an r.m.s. of 0.05 can we be reasonably sure of the validity of a two-component interpretation and then only for the last 10 or so oscillations, i.e. a signal-to-noise ratio (S/N) of at least about 30 is needed. This ratio applies to a two component signal - more components will demand even better S/Ns.

Another interesting application of the technique is to the sawtooth function $f_s(t) = \mathrm{rem}(t,t_R) - 1/2$, where t_R is the repetition time and $\mathrm{rem}(t,t_R)$ is defined as the remainder from division of t by t_R. f_s is discontinuous when $\mathrm{rem}(t,t_R) = 0$. A sample $N = 3000$ was constructed for $0 \leqslant t \leqslant 30$ comprising 30 teeth, i.e. $t_R = 100\ \Delta t$. Fig. 11 shows the resulting singular spectrum, from which it is not possible to infer how many components are present.

This difficulty is caused by undersampling of the switch-back phase of the sawtooth. Although this is a rather extreme example, spectra like these are the usual outcome of attempts to analyse data which are not sampled at a rate at least as fast as that suggested by Broomhead and King (1986). They advocate a Δt at least ten times shorter than the timescale corresponding to the smallest significant spectral content. Since the latter (even for smooth oscillations) typically corresponds to a timescale of P/10, this gives a bound $\Delta t \leqslant P/100$. A rather smaller Δt is desirable so that sub-samples with greater effective Δt may be constructed to verify that all the significant spectral content has been captured.

4.3 Application to DITE Data

Although much of the DITE soft X-ray data listed in Table I is apparently suitable for analysis on the basis of number of samples/oscillation, our experience above with $f_s(t)$ implies that the Broomhead-King method will not produce meaningful results. None of the discharges studied so far have sufficiently large $P/\Delta t$. Magnetic data collected prior to disruption on discharge 27512, sampled at $\Delta t = 2\mu s$, is suitable.

A data-set consisting of 2550 points was produced using coil 3 (see Fig. 4a), starting at $t = 509.5$ ms, and terminating 0.5 ms before the discharge disrupted at $t = 515.1$ ms. The singular spectrum, shown in Fig. 12a, can be demonstrated to be independent of $n \geqslant 4$ and effective Δt. However, it seems that the third largest component is significant, for the reconstruction in two-dimensions clearly intersects itself. The third component is however so noisy (c.f. the second component of the noisy f_e signal in Section 4.2) that a 3-D construction is useless. The Broomhead-King method therefore tells us only that $d_M > 2$. It is interesting that the noise level $\sim 10^{-2}$ is of the same order as the recording error in the data, i.e. the detectors (coils) are not responsible for the level of noise shown in the figure.

4.4 The Method as a Filter

Section 4.2, and in particular Fig. 10, have given the impression that the Broomhead-King technique is easily defeated by noise. However if one is seeking only to filter, i.e. reduce the noise content in a signal, the story is quite different. Indeed, the pedigree of the technique lies in the field of signal processing (Pike et al, 1984).

The drawback of the phase-space reconstruction technique is that components of intrinsically different size have to be given the same weight. However when the significant components are used to reconstruct the signal as a function of time, this is not so. The point is made by Fig. 13, for the noisy f_e data set. It is apparent that the two component reconstruction (bottom) is much smoother. The basic oscillation remains identifiable even though the $S/N \simeq 1$ for the first part of the data. Since the Broomhead-King method is very undemanding of computer time even for large samples, it clearly deserves attention as a filter, especially when little is known about the statistics of the noise affecting a signal.

5. Summary and Discussion

The main conclusion of the paper is provided by Tables VIII and IX, where are listed the data requirements for the four methods and their computational costs respectively, based on controlled studies of Lorenz system data. Broadly speaking there are two different types of requirement: the methods of Grassberger and Procaccia (1983b) and Wolf et al (1985) are much less demanding than those of Broomhead and King (1986) and Sano and Sawada (1985) in terms of both sampling rate and total sample size.

Of the four, the only one which we might not expect to give good results for DITE data is that of Broomhead and King (1986): it is defeated by the low precision (8-bit) at which measurements are recorded. Even so, it can provide a useful estimate of the complexity and noise content of signals. An application to JET data, which has higher precision, would be of interest.

Analysing DITE data, the first three methods perform rather worse than would be expected from the control studies, and we should like to understand why. One possibility is simply that the structure of the attracting trajectory in DITE discharges is more convoluted than that of the Lorenz system and hence the data requirements are more stringent. This is contradicted by the fact that we do get good estimates for the Grassberger and Procaccia exponent ν in the case of discharges 24591, 26246 and 28030, at least for larger values of the separation r. ν is the most robust of the three measures, but even so it is curious that especially in the latter two discharges, the r^{ν} line is followed for a relatively much smaller r-interval than in the control data-set, of which the truncation error was if anything larger than in the DITE data.

Is the kink in $C'(r)$ (see e.g. Fig. 5) due then to errors in measurement that are large enough to survive truncation? This seems unlikely for two reasons: (a) the Broomhead and King technique suggests any noise is smaller than the truncation error, and (b) the consistent form of the energy spectrum $E(\omega)$ at high frequency ω for the DITE signals. Fig. 14a, b and c show typical power spectra; the $E(\omega) \propto \omega^{-2.5}$ dependence apparently holds for all the discharges (except 24591 where the sampling is not fast enough and 27792 which is peculiar in other ways), at least to within the uncertainty ± 0.5 of measurement. In particular, discharge 27649 (Fig. 14c) shows the same feature, although no exponent ν could be assigned.

The indication is that there is a certain level of turbulence always present in DITE discharges. Superimposed on this we are seeing large-scale mode activity that can be explained in terms of a system with only a few degrees of freedom. The separation in amplitude between the two types of behaviour is sufficiently small that $C'(r)$ kinks and it is difficult to infer Lyapunov exponents reliably. Nevertheless the non-integer values of ν, plus the fact that one Lyapunov exponent is consistently positive all support the contention that the large-scale activity is chaotic and a strange attractor is present. The oddity of this result is that there is no reason why such a system of low degree should not yield the entire power spectrum in Fig. 14 (c.f. Fig. 14a and Fig. 14d).

It is possible to compare our dimensionality results with ones from TOSCA and JET (Coté et al, 1985; Robinson et al, 1986). Like Coté et al (1985), we find $\nu = 1 - 1.3$ for sawtooth oscillations in soft X-rays (DITE discharges 27649, 28030), that it is difficult to assign ν to the large amplitude irregular activity following disruptions (discharges 26246, part B, and 27792) and that steady state (flat top) discharges may have Mirnov activity resembling white noise (discharge 27649). The Mirnov signals from DITE discharges 26246 and 28030 which are modulated (albeit irregularly) at the frequency of the sawtooth have low ν only for $\log_{10} C > -1$, much as in corresponding JET discharges. However, in this range of C, DITE has $\nu \simeq 1.6 - 1.8$ compared to $\nu \simeq 1.3 - 1.4$ for JET. We have not so far found any DITE results that compare with the TOSCA or JET (notably Shot 3069, Robinson et al, 1986) findings of a $\nu \simeq 2.5$ over 3 factors of ten in C(r), for some of the higher amplitude, flat top Mirnov activity. Discharge 24591 is the only one for which C(r) has a constant logarithmic slope over a comparably sized interval.

To explain these latter discharges some form of nonlinear MHD modelling, perhaps using the FORBAK code (Eastwood and Arter, 1986), might well be fruitful. It is likely that these interactions fit the pattern of "weak" turbulence, where only a few modes interact to give irregular behaviour, as shown in hydrodynamic experiments by Brandstater et al (1983) and Guckenheimer and Buzyna (1983).

We note particularly also the recent work of Ciliberto and Gollub (1985a,b) where a phenomenological model is found to reproduce many of the features of a surface wave experiment including approximately the same ν. While it is clear that relatively simple nonlinear dynamical systems can reproduce even quite violent, irregular, bursty behaviour (e.g. Fig. 4 of Fujisaka and Yamada, 1985), little attention has been paid to systems which may have a significant non-deterministic component, such as are represented by the other types of discharge.

Acknowledgements

We are grateful to Messrs. K.B. Axon and W. Millar for providing the DITE data, and to Drs. J.W. Eastwood, J. Hugill and P.C. Johnson for their encouragement. We also acknowledge helpful discussions with Dr. D.S. Broomhead of R.S.R.E.

Table I

Descriptions of data-sets studied

Data-set	Characteristic time(s) ms	Sample interval ms	Samples/ Oscillation	Size
Lorenz (Section 2)	0.75 (dimensionless)	0.1 (dimensionless)	7.5	2000
DITE discharge 24591	0.1-0.2 (Magnetic)	.025	8-16	1920
DITE discharge 26246(part A)	0.1 (Magnetic)	.010	10	1800
DITE discharge 27649	0.3,4 (SXR) 0.1 (Magnetic)	.005	60,400 20	3894
DITE discharge 27792	0.01,0.3 (Magnetic)	.002	5,150	2046
DITE discharge 28030	0.05-0.1,2 (SXR) 0.1 (Magnetic)	.010	5-10,200 10	2700
Lorenz, r_L=40 (Section 3)	0.5	.035	14	4000
Lorenz, r_L=45.92 (Section 3)	0.45	0.1	4.5	1998
DITE discharge 27512	0.1-0.3 (Magnetic)	.002	50-150	2550

Table II

a) SS method applied to c(t) from Lorenz equations (2.3), $\sigma_L = 16$, $r_L = 40$ and $\ell_L = 4$. N = 4000, λ_i = (1.37,0.00, -22.37) (Shimada and Nagashima, 1979). $N_e(\tau, \theta) = N\Delta t/\theta$ measures how many estimates of the λ_i are averaged to give the values in the final column. Underlined λ_i indicates apparent convergence, otherwise the final iterate is given.

Run	ε	$\tau/\Delta t$	$\theta/\Delta t$	M	N_e	λ_i		
1	.025	3	2	3	2000	6,	-0.6,	-6
2	.025	3	2	4	2000	3.7,	-1,	-15
3	.025	3	2	6	2000	2.8,	-1,	-15
4	.025	3	2	15	2000	2.8,	-1,	-17
5	.015	3	2	6	2000	5,	-2,	-32
6	.05	3	2	6	2000	2.4,	-1.1,	-14
7	.05	3	2	15	2000	2.0,	-0.8,	-16
8	.05	3	1	15	4000	2.5,	-1.3,	-23
9	.05	3	3	15	1300	1.6,	-0.4,	-10
10	.05	3	4	15	1000	1.8,	-0.3,	-6
11	.05	3	5	15	800	2.0,	0.07,	-4.5
12	.05	3	8	15	500	2.4,	0.5,	-3
13	.05	3	10	15	400	2.8,	1.0,	-1
14	.05	3	20	15	200	2.0,	1.0,	-0.5
15	.05	1	4	15	1000	2.5,	-0.2	-6
16	.05	2	4	15	1000	2.0,	-0.2,	-6
17	.05	4	4	15	1000	1.8,	-0.4,	-4.6
18	.05	5	4	15	1000	1.6,	-0.2,	-6
19	.05	7	4	15	1000	4.1,	-0.3,	-6
20	.05	11	4	15	1000	3.2,	0.1,	-5

b) As (a), but using a(t) from the Lorenz equations.

Run	ε	$\tau/\Delta t$	$\theta/\Delta t$	M	N_e	λ_i		
1	.025	3	2	3	2000	4.7,	-0.4,	-20
2	.05	3	1	15	4000	1.2,	0.1,	-23
3	.05	3	2	15	2000	1.3,	0.0,	-18
4	.05	3	4	15	1000	1.2,	0.0,	-9
5	.05	3	5	15	800	1.4,	0.1,	-6
6	.05	1	2	15	2000	1.8,	-0.8,	-21
7	.05	2	2	15	2000	1.5,	-0.2,	-20
8	.05	5	2	15	2000	1.7,	-0.2,	-19
9	.05	7	2	15	2000	3.9,	-0.4,	-12

Table III

Lyapunov exponents (in units of ms^{-1}) from SS method applied to

(a) Magnetic signal from discharge 28030, n = 2

$\tau/\Delta t$ $\theta/\Delta t$ =	1	2
1	21, -65	19, -32
2	27, -59	19, -26
3	44, -44	24, -19

(b) As (a); but with n = 3

$\tau/\Delta t$ $\theta/\Delta t$ =	1	2
1	41, -5, -75	33, 3.5, -43
2	62, 14, -59	25, 2, -30
3	83, 26, -58	43, 16, -32

(c) As (a); but with n = 4

$\tau/\Delta t$ $\theta/\Delta t$ =	1	2
1	35, 11, -4, -25	27, 13, 1.5, -16
2	66, 40, 19, -16	20, 7, -0.8, -15
3	75, 46, 24, -13	39, 24, 14, -4

(d) Magnetic signal from discharge 24591, coil 1, n = 3

$\tau/\Delta t$ $\theta/\Delta t$ =	1	2
1	12, -3, -26	11, -0.5, -18
2	18, -1, -34	7, -1.5, -14

(e) Magnetic signal from discharge 24591, coil 4, n = 3

$\tau/\Delta t$ $\theta/\Delta t$ =	1	2
1	20, 0, -25	17, 3, -14
2	36, 14, -23	15, 1.2, -12

Table IV

WSSV method applied to c(t) from Lorenz equations (2.3), $\sigma_L = 16$, $r_L = 45.92$ and $\ell_L = 4$. $\lambda_1 = 2.16$

Run	ε	ε_{in}	$\tau/\Delta t$	$\theta/\Delta t$	N_e	λ_1
(a) n = 3						
1	0.05	0.005	1	1	2000	2.1
2	0.05	0.005	1	2	1000	2.1
3	0.05	0.005	1	4	500	2.0
4	0.05	0.005	1	6	330	2.0
5	0.05	0.005	1	8	250	1.8
6	0.05	0.005	2	4	500	1.9
7	0.05	0.005	3	4	500	2.1
8	0.05	0.005	4	4	500	1.8
9	0.05	0.005	5	4	500	2.4
10	0.05	0.005	6	4	500	2.3
11	0.05	0.005	8	4	500	2.5
12	0.05	0.005	2	1	2000	2.6
13	0.05	0.005	4	1	2000	3.1
14	0.05	0.005	6	1	2000	4.4
15	0.02	0.002	2	4	500	2.0
16	0.02	0.002	2	6	330	2.1
17	0.02	0.002	2	8	250	1.9
18	0.02	0.002	3	4	500	2.2
19	0.02	0.002	3	6	330	1.8
20	0.02	0.002	3	8	250	1.9
21	0.02	0.002	4	4	500	2.0
22	0.02	0.002	4	6	330	2.0
23	0.02	0.002	4	8	250	1.8
(b) n = 4						
24	0.02	0.002	2	4	500	1.8
25	0.02	0.002	4	4	500	1.7
26	0.02	0.002	6	4	500	1.8
27	0.02	0.002	8	4	500	2.2
(c) n = 5						
28	0.02	0.002	2	4	500	1.8
29	0.02	0.002	4	4	500	1.4
30	0.02	0.002	6	4	500	1.7

Table V

Largest Lyapunov exponent (in units of ms^{-1}) from WSSV method applied to

(a) Magnetic signal from discharge 24591, coil 1, n = 3

$\tau/\Delta t$ $\theta/\Delta t$ =	2	3	4	6	10
1	11	9	9	7	5.5
3	10	5	5.5	4	3.5
5	13	11	7	5.5	3.6
7	17	9	6.5	7	3.0

(b) As (a) above, but n = 4

$\tau/\Delta t$ $\theta/\Delta t$ =	2	3	4	6	10
1	7	5	5	4.5	3.5
3	5.5	3.5	4	3	2.0
5	6.5	5	3.5	2.7	2.1
7	11	4	4.5	4	2.0

Table VI

Largest Lyapunov exponent (in units of ms^{-1}) from WSSV method applied to

(a) Magnetic signal from Part A of discharge 26246, coil 1, n = 3

$\tau/\Delta t$ $\theta/\Delta t$ =	2	3	4	7	12
1	34	33	27	17	12
3	34	16	20	12	10
5	50	35	25	18	11
7	45		26	10	11

(b) As (a), but n = 4

$\tau/\Delta t$ $\theta/\Delta t$ =	2	3	4	7	12
1	21	19	17	13	9
3	16	11	12	8	6
5	27	19	15	11	7
7	22	15	12	6	6

Table VII

Largest Lyapunov exponent (in units of ms^{-1}) from WSSV method applied to

(a) Magnetic signal from discharge 28030, n = 3

$\tau/\Delta t$ $\theta/\Delta t$ =	2	3	4	7	12
1	44	40	29	18	12.5
3	52	18	28	17	11
5		50	34	21	15
7		38	28	12	12

(b) As (a), but n = 4

$\tau/\Delta t$ $\theta/\Delta t$ =	2	3	4	7	12
1	26	20	19	12	8
3	27	12	16	11	8
5	41	29	22	15	11
7			14	7	8

Table VIII

Estimates of requirements and parameters for the data analysis techniques
(N/A denotes not an applicable parameter to that method)

Technique	No. of oscns	Samples/ oscn	S/N	τ	n	N	θ	ε_{in}	ε	M
Grassberger & Procaccia	$10^{\nu-1}$ - $100^{\nu-1}$	≥ 6	$\geq$ 8-bit precision	$0\left(\frac{P}{n}\right)$	$[\nu]+3 \geq n \geq [\nu]$*	$10^{\nu}-30^{\nu}$	N/A	N/A	N/A	N/A
Wolf et al+	$10^{\nu-1}$ - $100^{\nu-1}$	$\geq[\nu]$	$\geq$ 8-bit precision	$0\left(\frac{P}{n}\right)$	$[\nu]+3 \geq n$	$10^{\nu}-30^{\nu}$	$\frac{P}{2} - \frac{3P}{2}$	0.005	0.05	N/A
Sano & Sawada	$10^{\nu-1}$ - $100^{\nu-1}$	$\geq$15	$\geq$ 8-bit precision	$<\min\left(\frac{P}{3}, 2\theta\right)$	$\max([\nu], 3)$	$10^{\nu+1}-30^{\nu+1}$	$< \frac{P}{3}$	0	0.05	$\geq$15
Broomhead & King	$10^{\nu-1}$ - $100^{\nu-1}$	$\geq$10n	$\leq 10^{-[\nu]}$	$0\left(\frac{P}{10n}\right)$	$n \geq 2[\nu]+1$	$10^{\nu+1}-30^{\nu+1}$	N/A	N/A	N/A	N/A

+See the discussion in Wolf et al (1985).

*$[\nu]$ is defined to be the first integer greater than ν.

Table IX

Computational Costs of the Data Analysis Techniques

Technique	Indicative parameters	Typical cost (CRAY seconds)	Scaling
Grassberger & Procaccia	N = 2000, n = 4	8*	nN^2
Wolf et al	N = 2000, p = 4, n = 3	10	nN^2p^{-1}**
Sano & Sawada	N = 4000, p = 2, n = 3,(M = 4)	43	nN^2p^{-1}**
Broomhead & King	N = 3000, n = 10	1***	n^2N

*Code for calculating ν employs CRAY masking and merging routines. Other computations performed using FORTRAN 77 only.

**N^2 scaling assumes whole data-set needs to be searched to find M near neighbours (in the SS case) or a single close neighbour (in the WSSV method). This may be a gross overestimate for some data for which a scaling with N-exponent closer to one might be more appropriate.

***Takes 7s on PRIME 9950.

References

W. Arter and D.N. Edwards, 1985, "Dimensionality and MHD mode coupling studies of DITE", pp.442-445 in Proc. 12th European Conf. Controlled Fus. and Plasma Phys. Vol.II (L. Pocs and A. Montvai eds.), E.P.S.

W. Arter and D.N. Edwards, 1986, "Non-linear studies of Mirnov oscillations in the DITE tokamak: evidence for a strange attractor", Phys. Lett. 114A, 84-89.

R. Badii and A. Politi, 1984, "Hausdorff dimension and uniformity factor of strange attractors", Phys. Rev. Lett. 52, 1661-1664.

A. Ben-Mizrachi, I. Procaccia and P. Grassberger, 1984, "Characterisation of experimental (noisy) strange attractors", Phys. Rev. A29, 975-977.

A. Brandstater, J. Swift, H.L. Swinney, A. Wolf, J.D. Farmer, E. Jen and P.J. Crutchfield, 1983, "Low-dimensional chaos in a hydrodynamic system", Phys. Rev. Lett. 51, 1442-1445.

D.S. Broomhead and G.P. King, 1986, "Extracting qualitative dynamics from experimental data", Physica D (submitted).

S. Ciliberto and J.P. Gollub, 1985a, "Chaotic mode competition in parametrically forced surface waves", J. Fluid Mech. 158, 381-398.

S. Ciliberto and J.P. Gollub, 1985b, "Phenomenological model of chaotic mode competition in surface waves", Il Nuovo Ciment. 6D, 309-316.

A. Coté, P. Haynes, A. Howling, A.W. Morris and D.C. Robinson, 1985, "Dimensionality of fluctuations in TOSCA and JET", pp.450-453 in Proc. 12th European Conf. Controlled Fus. and Plasma Phys. Vol.II (L. Pocs and A. Montvai eds.), E.P.S.

J.W. Eastwood and W. Arter, 1986, "Reduced MHD modelling of tearing mode interactions in tokamaks", CLM-P779, submitted to Phys. Fluids.

J.-P. Eckmann and D. Ruelle, 1985, "Ergodic theory of chaos and strange attractors", Rev. Mod. Phys. 57, 617-656.

P. Frederickson, J.L. Kaplan, E.D. Yorke and J.A. Yorke, 1983, "The Lyapunov dimension of strange attractors", J. Diff. Equ. 49, 185-207.

H. Fujisaka and T. Yamada, 1985, "A new intermittency in coupled dynamical systems", Prog. Theor. Phys. 74, 918-921.

P. Grassberger and I. Procaccia, 1983a, "Characterisation of strange attractors", Phys. Rev. Lett. 50, 346-349.

P. Grassberger and I. Procaccia, 1983b, "Measuring the strangeness of strange attractors", Physica 9D, 189-208.

P. Grassberger and I. Procaccia, 1983c, "Estimation of the Kolmogorov entropy from a chaotic signal", Phys. Rev. A28, 2591-2593.

J. Guckenheimer and G. Buzyna, 1983, "Dimension measurements for geostrophic turbulence", Phys. Rev. Lett. 51, 1438-1441.

E.N. Lorenz, 1963, "Deterministic nonperiodic flow", J. Atmos. Sci. 20, 130-141.

B.B. Mandelbrot, 1977, Fractals: Form, Chance and Dimension, Freeman.

C. Nicolis and G. Nicolis, 1984, "Is there a climatic attractor?", Nature 311, 529-532.

E. Ott, W.D. Withers and J.A. Yorke, 1984, "Is the dimension of chaotic attractors invariant under coordinate changes?", J. Stat. Phys. 36, 687-697.

E.R. Pike, J.G. McWhirter, M. Bertero and C. de Mol, 1984, "Generalised information theory for inverse problems in signal processing", IEE Proc. 131F, 660-667.

D.C. Robinson, P. Haynes and A.W. Morris, 1986, "MHD activity on JET", JET-P(85)11, presented at Workshop on Magnetic Reconnection and Turbulence, Cargese.

M. Sano and Y. Sawada, 1985, "Measurement of the Lyapunov spectrum from a chaotic time series", Phys. Rev. Lett. 55, 1082-1085.

I. Shimada and T. Nagashima, 1979, "A numerical approach to ergodic problem of dissipative dynamical systems", Prog. Theor. Phys. 61, 1605-1616.

F. Takens, 1981, "Detecting strange attractors in turbulence", pp.366-381 in Dynamical Systems and Turbulence (D.A. Rand and L.-S. Young eds.), Springer.

Y. Termonia and Z. Alexandrowicz, 1983, "Fractal dimension of strange attractors from radius versus size of arbitrary clusters", Phys. Rev. Lett. 51, 1265-1268.

A. Wolf, J.B. Swift, H.L. Swinney and J.A. Vastano, 1985, "Determining Lyapunov exponents from a time series", Physica 16D, 285-317.

L.-S. Young, 1982, "Dimension, entropy and Lyapunov exponents", Ergod. Th. Dynam. Sys. 2, 109-124.

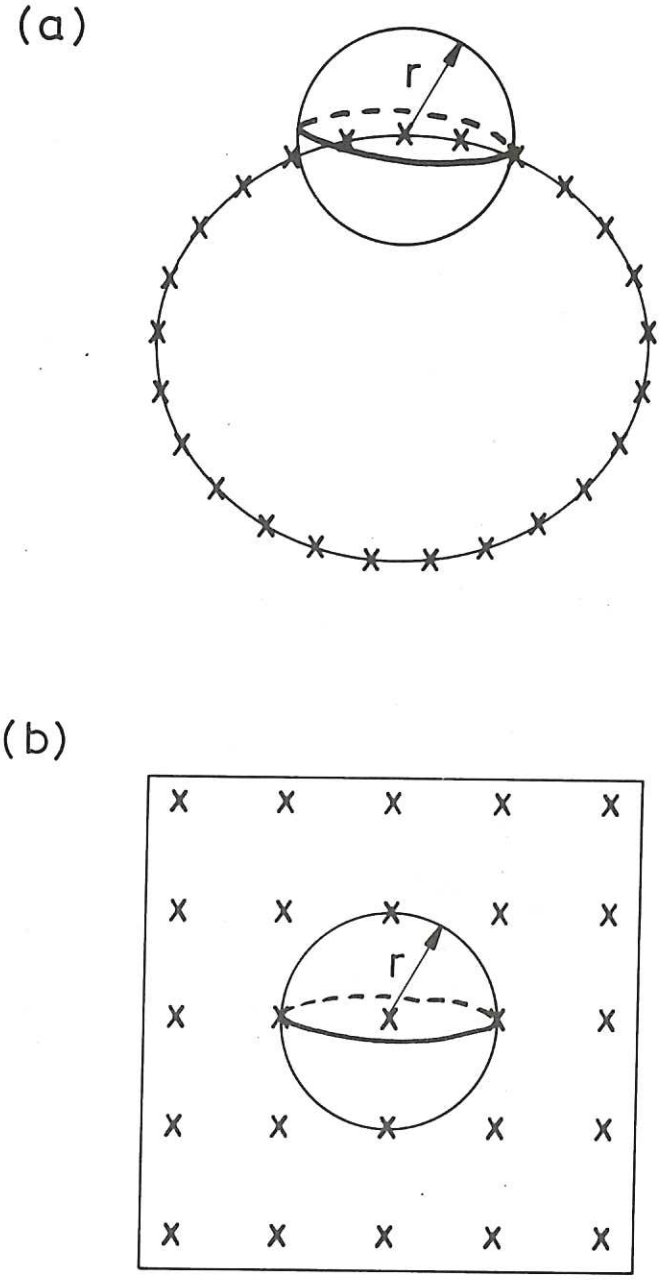

Fig. 1 The Grassberger and Procaccia exponent ν equals the dimension of everyday objects: (a) for the perimeter of an ellipse, the number of points within a radius ν of a given one increases proportionately as r, (b) for the square sheet, a quadratic dependence is obtained.

CLM-R269

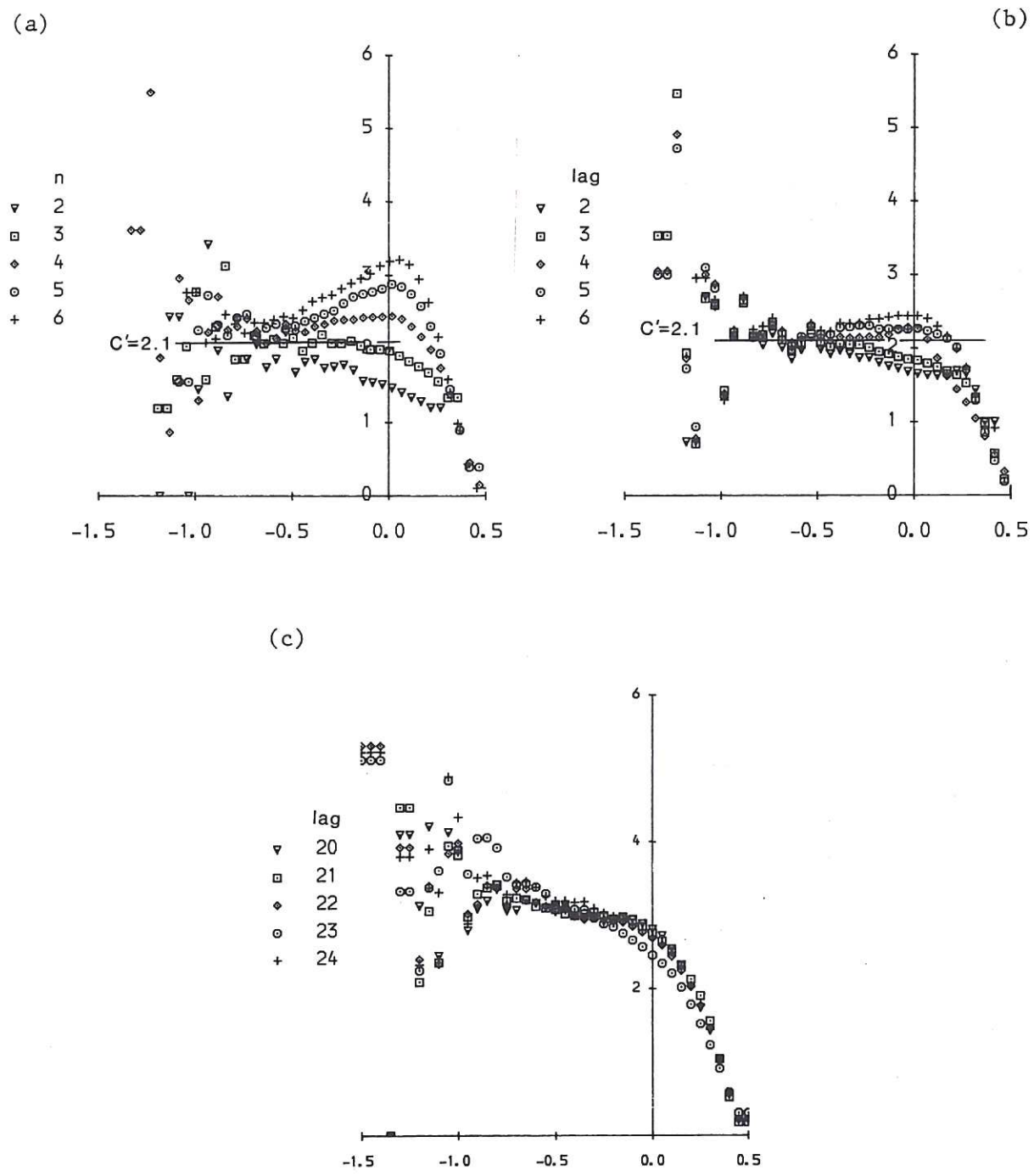

Fig. 2 $C'(r) = d \log C / d \log(r/r_o)$ plotted against $\text{lag}_{10(r/ro)}$ for the c-component of the Lorenz system (2.3) at parameters listed in Chapter 2. (a) is drawn for varying dimension n as indicated in the legend ($\tau/\Delta t = 6$), while (b) and (c) are for varying values of the lag-time $\tau/\Delta t$ recorded in the legend (n = 4).

CLM-R269

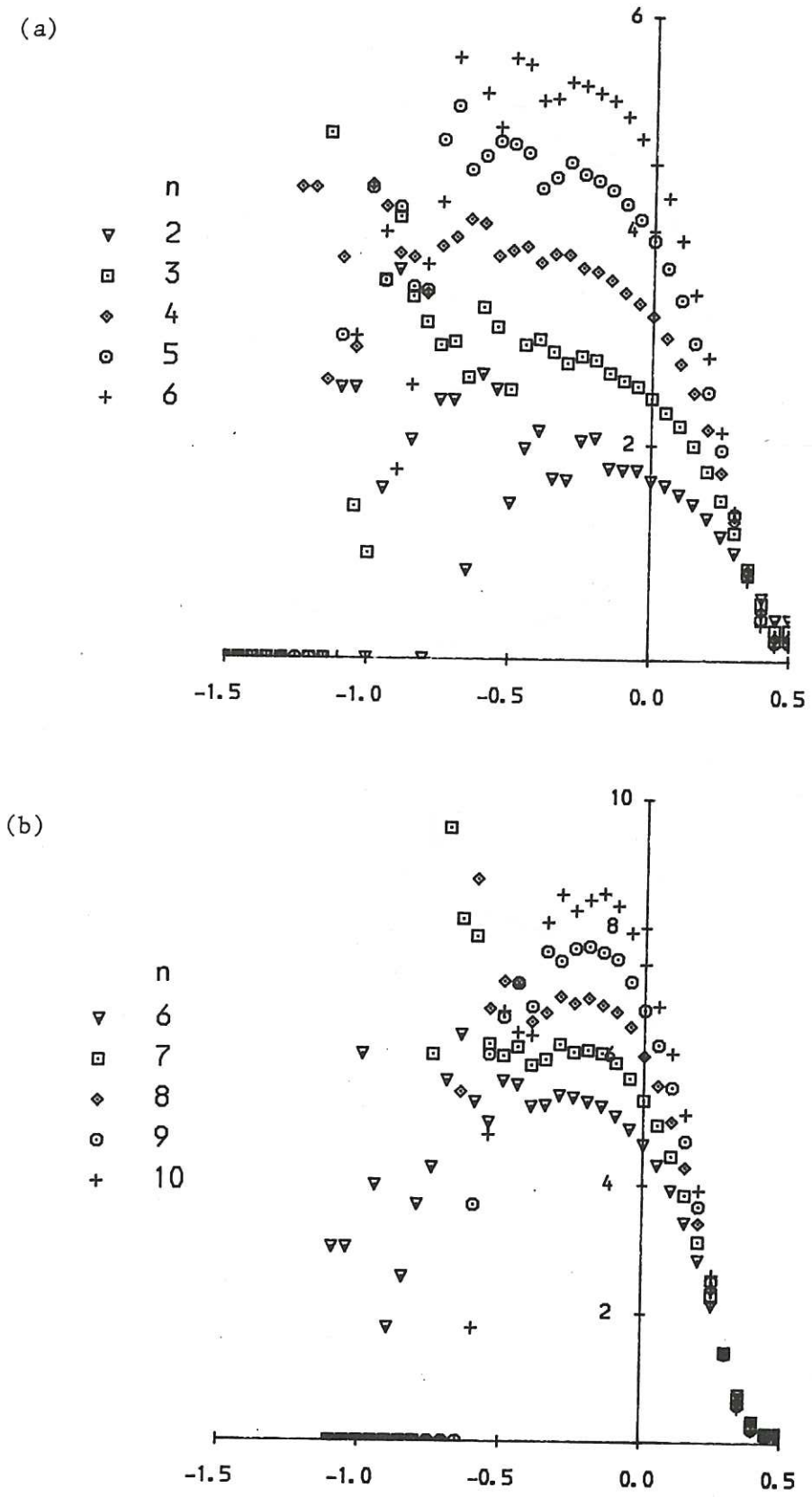

Fig. 3 C′(r) plotted against $\log_{10}(r/r_o)$ for random data: (a) for dimensions $2 \leq n \leq 6$, (b) for dimensions $6 \leq n \leq 10$.

CLM-R 269

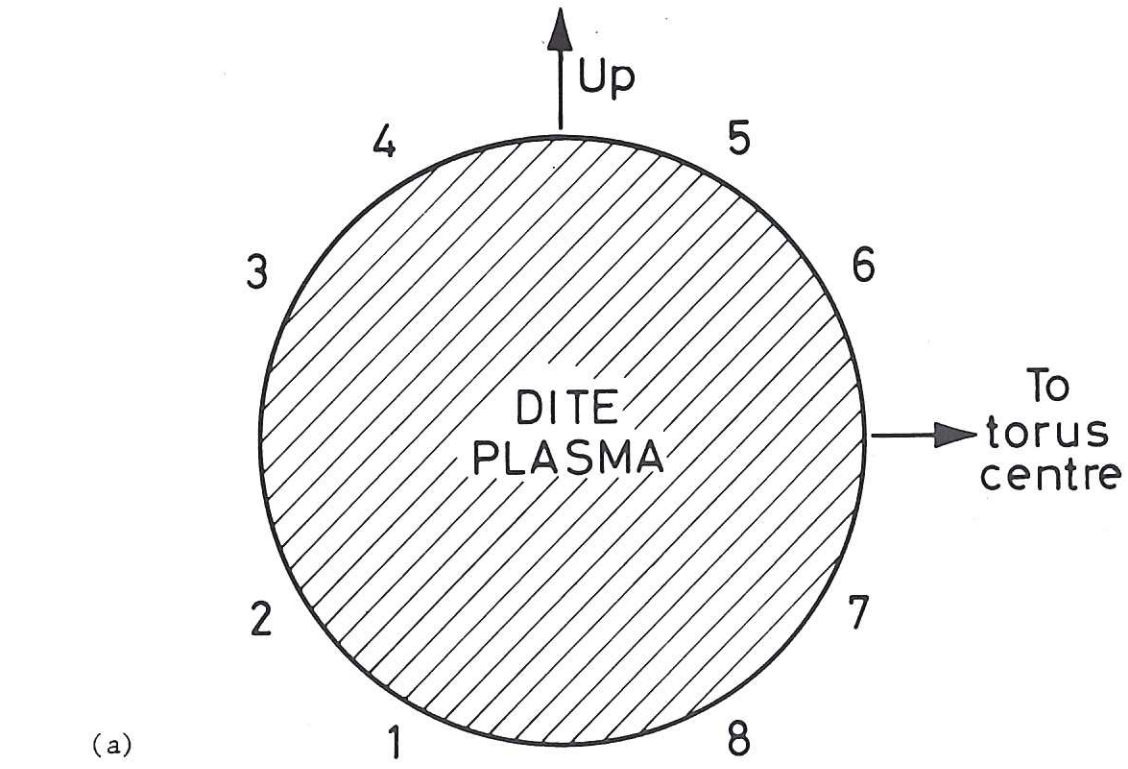

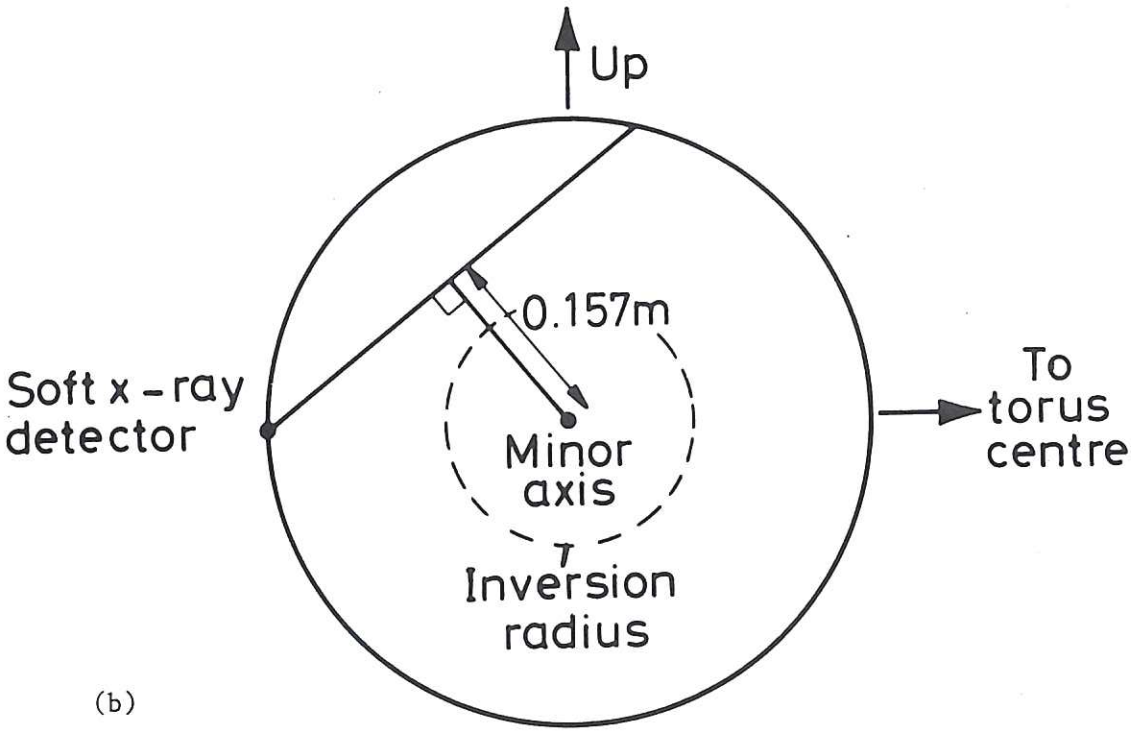

Fig. 4 Situation of DITE diagnostics in tokamak minor cross-section: (a) the numbers mark the locations of the Mirnov coils which lie inside the vacuum vessel, (b) shows the line of sight from which soft X-ray signals from discharge 27649 were collected and analysed.

CLM-R269

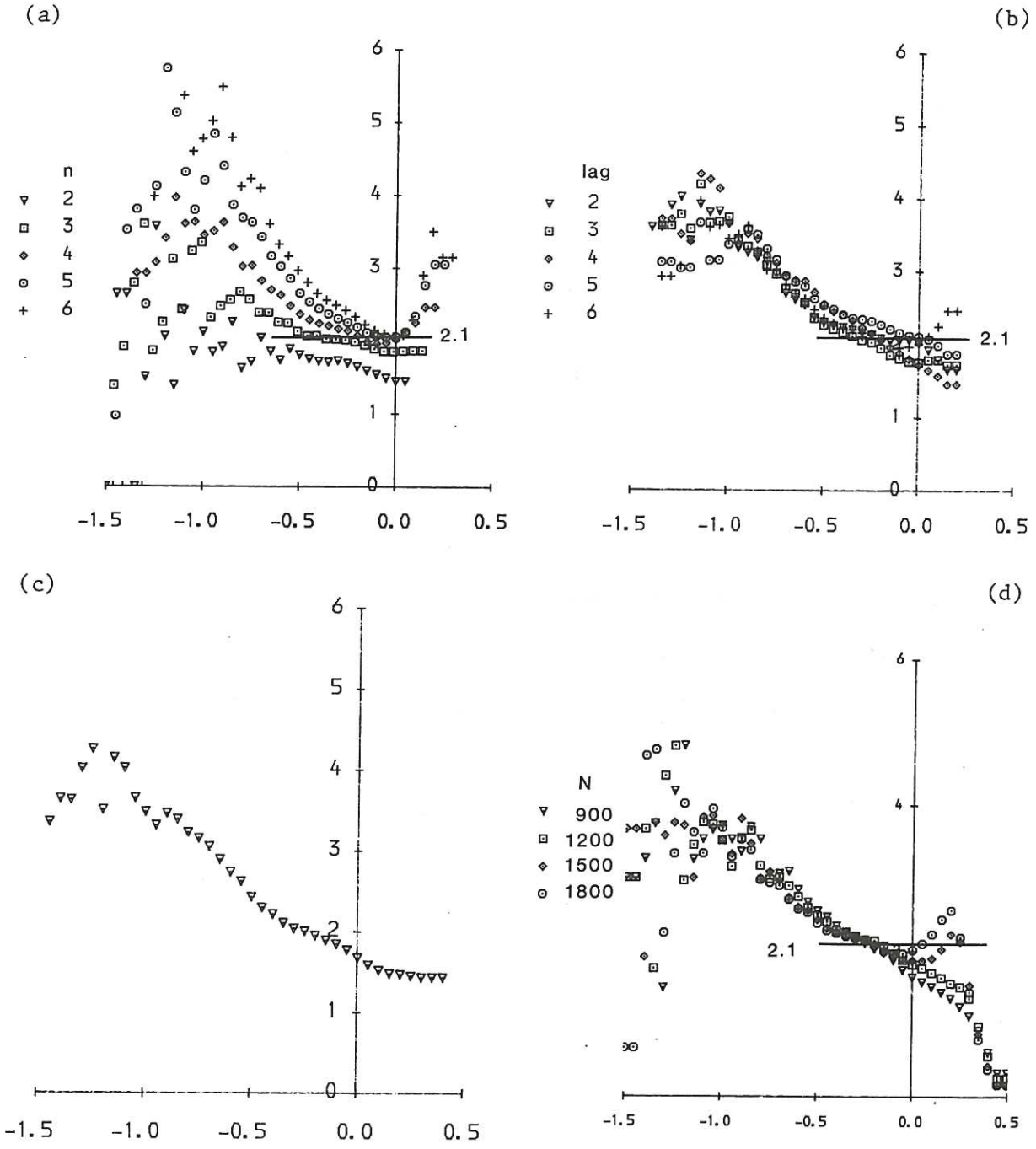

Fig. 5 $C'(r) = d\ \log C / d\ \log(r/r_o)$ plotted against $\log_{10}(r/r_o)$ for coil 1 of DITE discharge 24591: (a) is drawn for varying dimension n as indicated in the legend ($\tau/\Delta t = 6$), (b) for varying τ (n = 4) and (d) for varying sample size N(n = 4 and $\tau/\Delta t = 6$). (c) is drawn for 4-dimensional vectors constructed out of the signals from coils 1, 2, 3 and 4.

CLM-R269

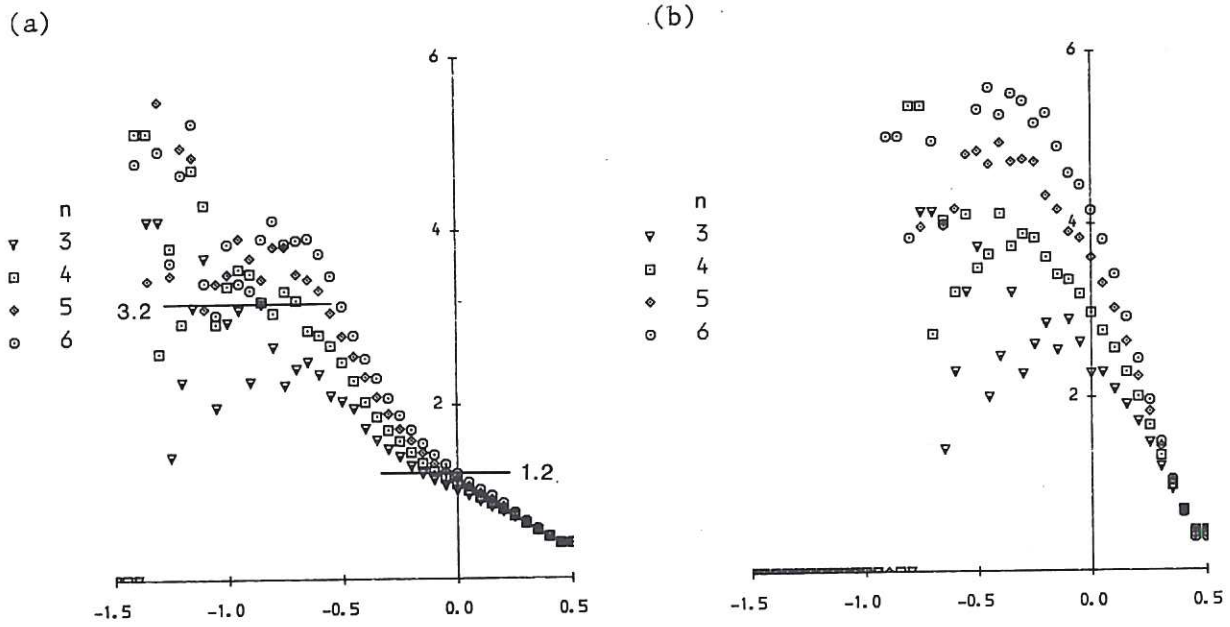

Fig. 6 C′(r) plotted against $\log_{10}(r/r_o)$ for (a) soft X-ray signals and (b) Mirnov data from DITE discharge 27649. $\tau/\Delta t=4$ and the varying dimension n is indicated in the legend.

CLM-R269

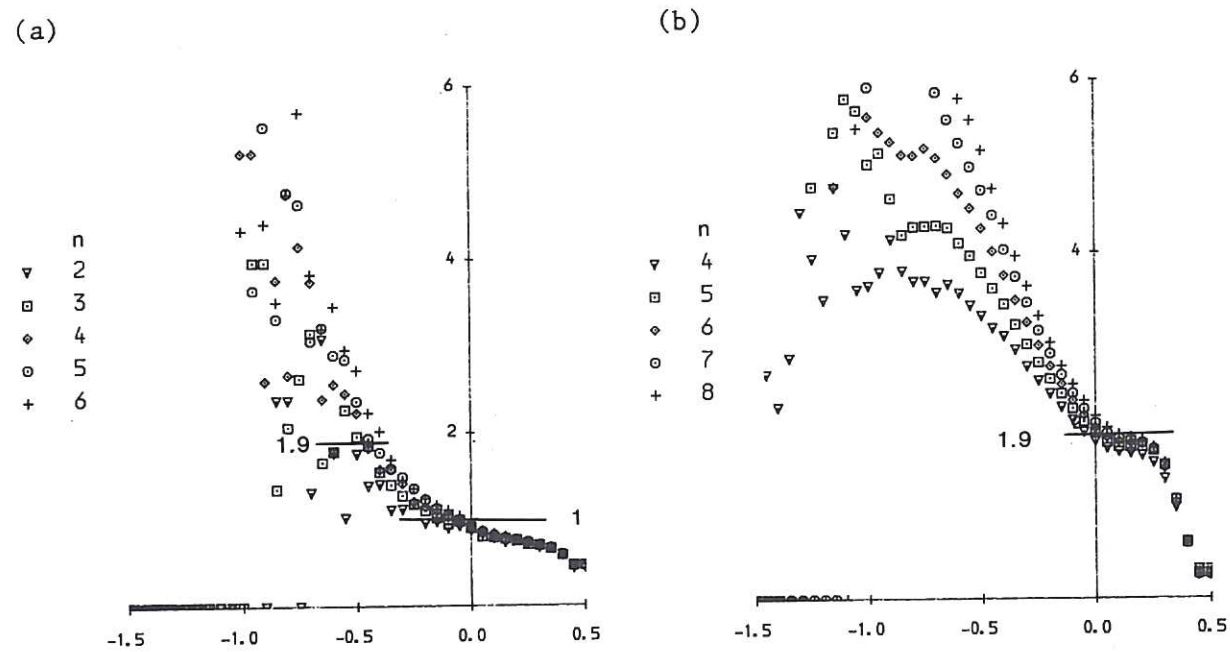

Fig. 7 C′(r) plotted against $\log_{10}(r/r_o)$ for (a) soft X-ray signals and (b) Mirnov data from DITE discharge 28030. $\tau/\Delta t=2$ and the varying dimension n is indicated in the legend.

CLM-R269

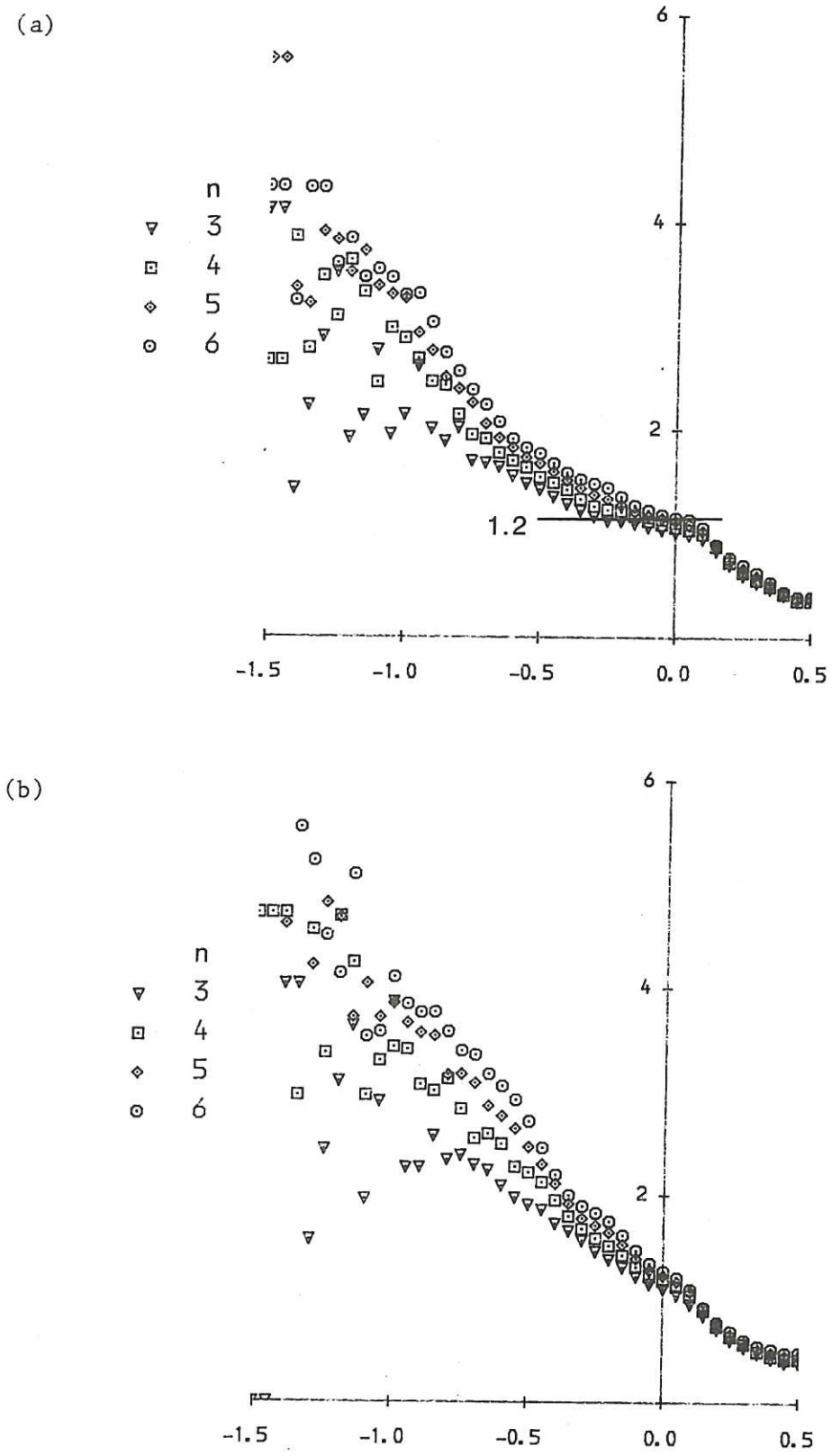

Fig. 8 C′(r) plotted against $\log_{10}(r/r_o)$ for magnetic data from (a) coil 5 and (b) coil 7 for DITE discharge 27792. $\tau/\Delta t=4$ and the varying dimension n is indicated in the legend

CLM-R269

(a)

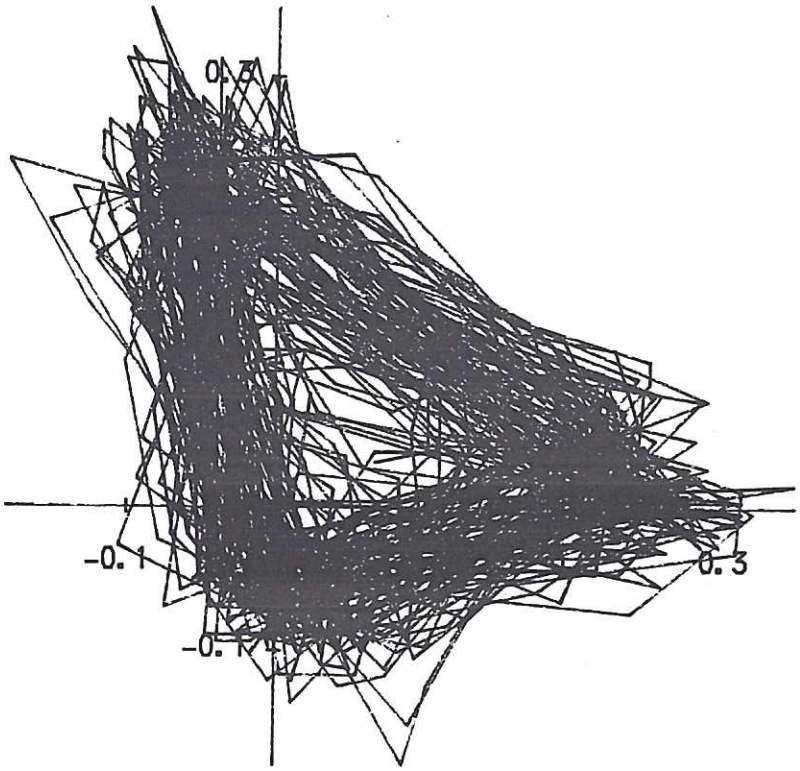

(b)

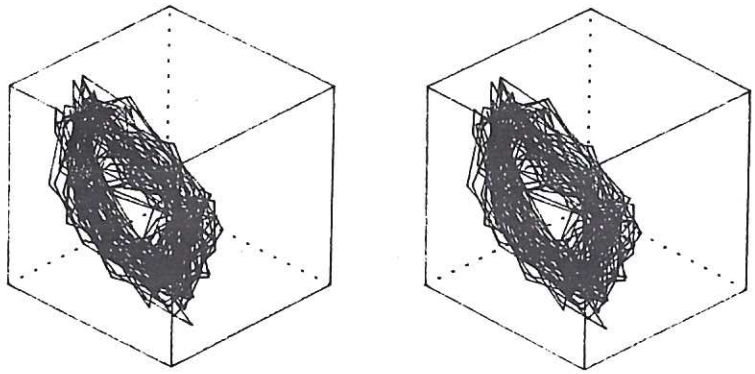

Fig. 9 Delay co-ordinate space reconstructions of the Mirnov signal X(t) (in arbitrary units) from discharge 28030. (a) shows X(t) plotted versus $X(t+\tau)$ where $\tau = 3\Delta t$ (for clarity only the first 1000 points are shown) and (b) shows points $(X(t), X(t+\tau), X(t+2\tau))$, $\tau = 7\Delta t$, joined in 3 dimensional space (only the first 500 such points are shown). (b) is drawn for stereoscopic viewing. This may be done using any of the usual stereoscopic viewers or, without such paraphernalia, by relaxing the eye focussing muscles, letting each eye look at only one drawing. (To achieve this decoupling, it may be helpful to place a card vertically between the eyes, parallel with the nose, in order to cut off the left-hand drawing from the sight of the right eye, and vice-versa). Those who have neither the equipment nor sufficient ocular accommodation may simply consider the diagram as being duplicated.

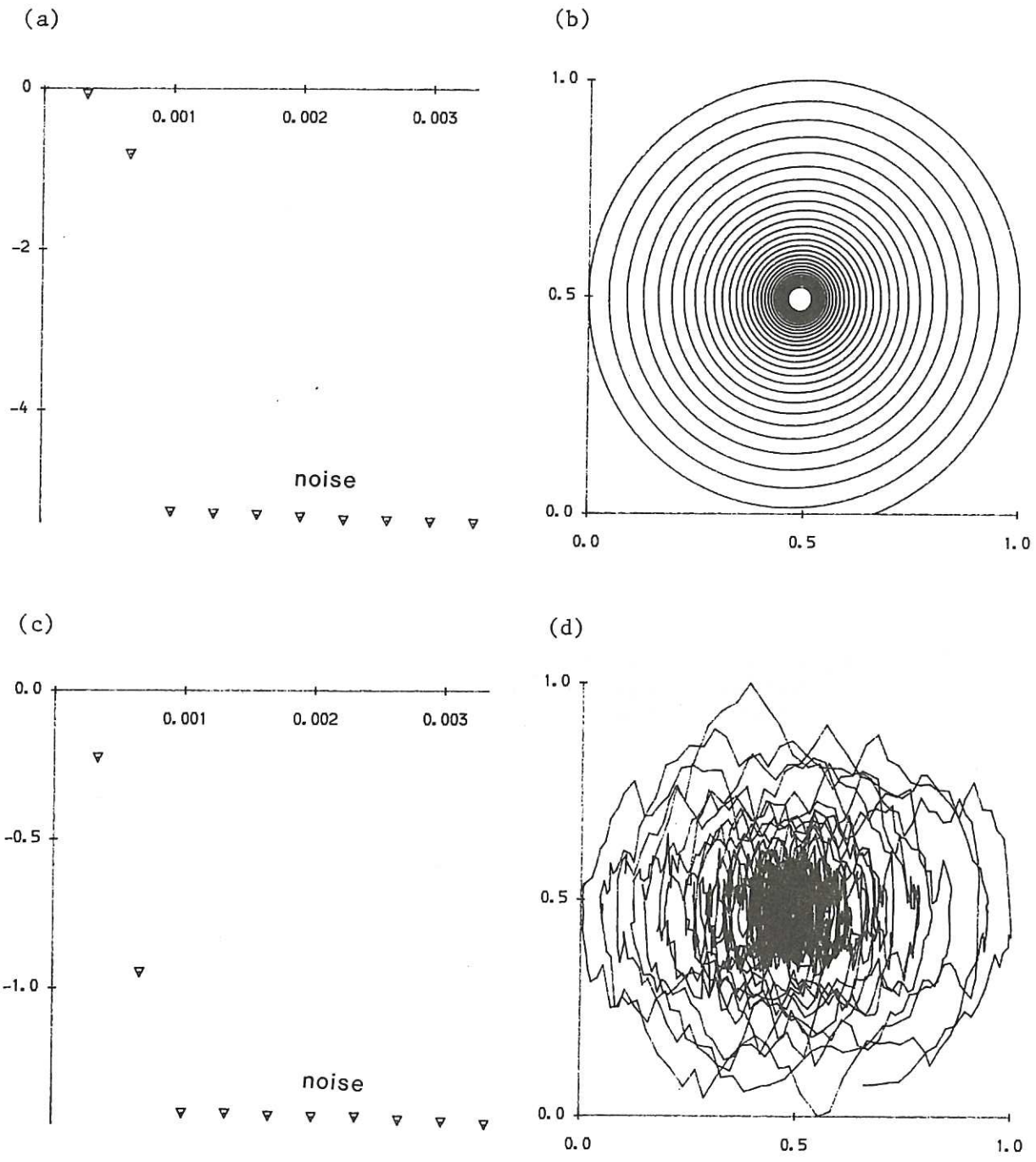

Fig. 10 The growing oscillation $f_e(t)$ of Section 4.2 analysed by the Broomhead-King method: (a) shows the singular spectrum, a plot of $\log_{10}(\sigma_i/\sigma_0)$ versus $i\tau$, where $\tau=\Delta t$ and an embedding dimension $n=10$ has been used. (b) shows the 2-D phase space reconstruction, P_2 plotted versus P_1 where the projections $P_i=\underset{\approx}{T}\underset{\sim}{c_i}$, $i=1, 2$, correspond to the two largest σ_i shown in part (a). $\sigma_0=\sum_{i=1}^{n}\sigma_i$ is a convenient normalisation for σ_i and the projections are scaled so as to fit the unit interval. (c) and (d) are as (a) and (b), except that more noise has been deliberately added to the signal as described in Section 4.2

CLM-R269

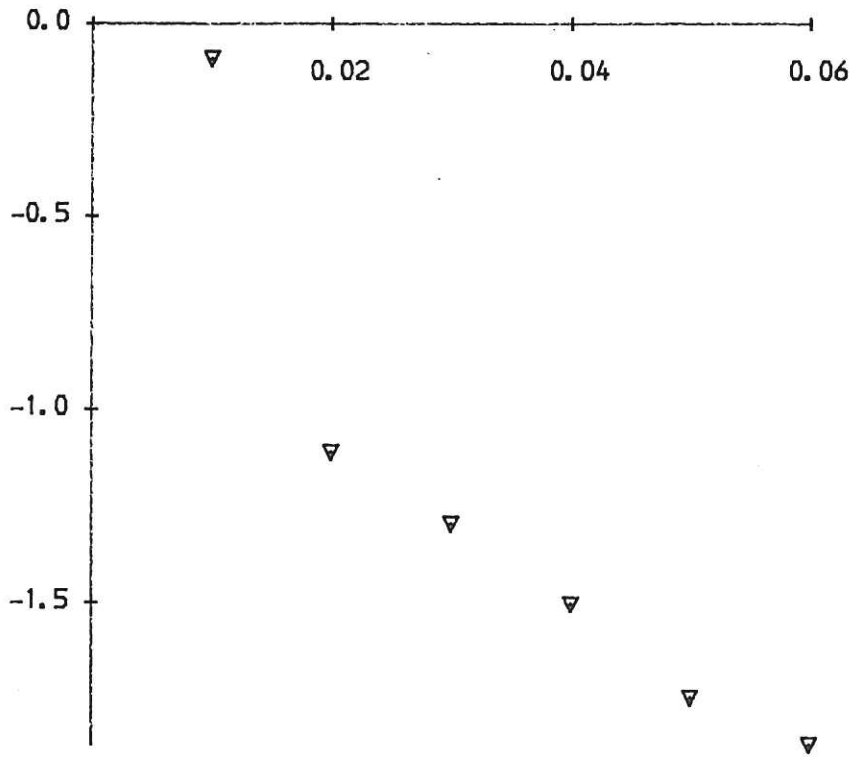

Fig. 11 The singular spectrum, $\log_{10}(\sigma_i/\sigma_o)$ plotted versus $i\tau$, for the sawtooth function $f_s(t)$ of Section 4.2, $\tau=\Delta t$ and $n=10$ were used - there is no indication that the spectrum is resolved.

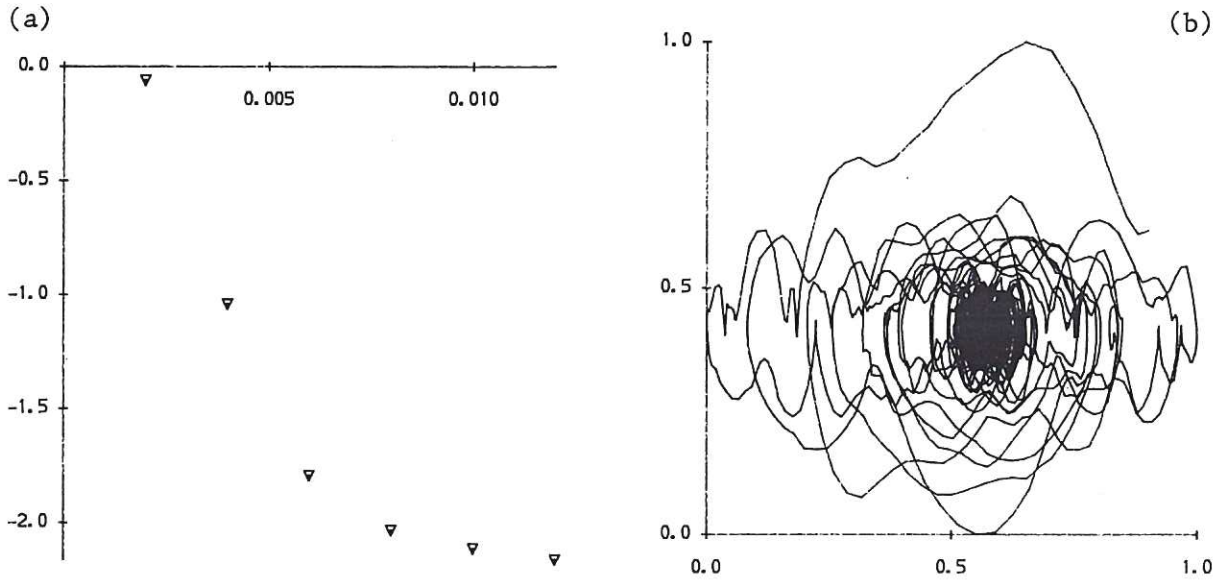

Fig. 12 (a) The singular spectrum, $\log_{10}(\sigma_i/\sigma_o)$ plotted versus $i\tau$, for the Mirnov signal from DITE discharge 27512. $\tau=\Delta t$ and $n=6$ were used.

(b) 2-D phase space reconstruction of the signal from discharge 27512, using the (scaled) projections P_1 and P_2 corresponding to the two largest σ_i shown in part (a).

CLM-R 269

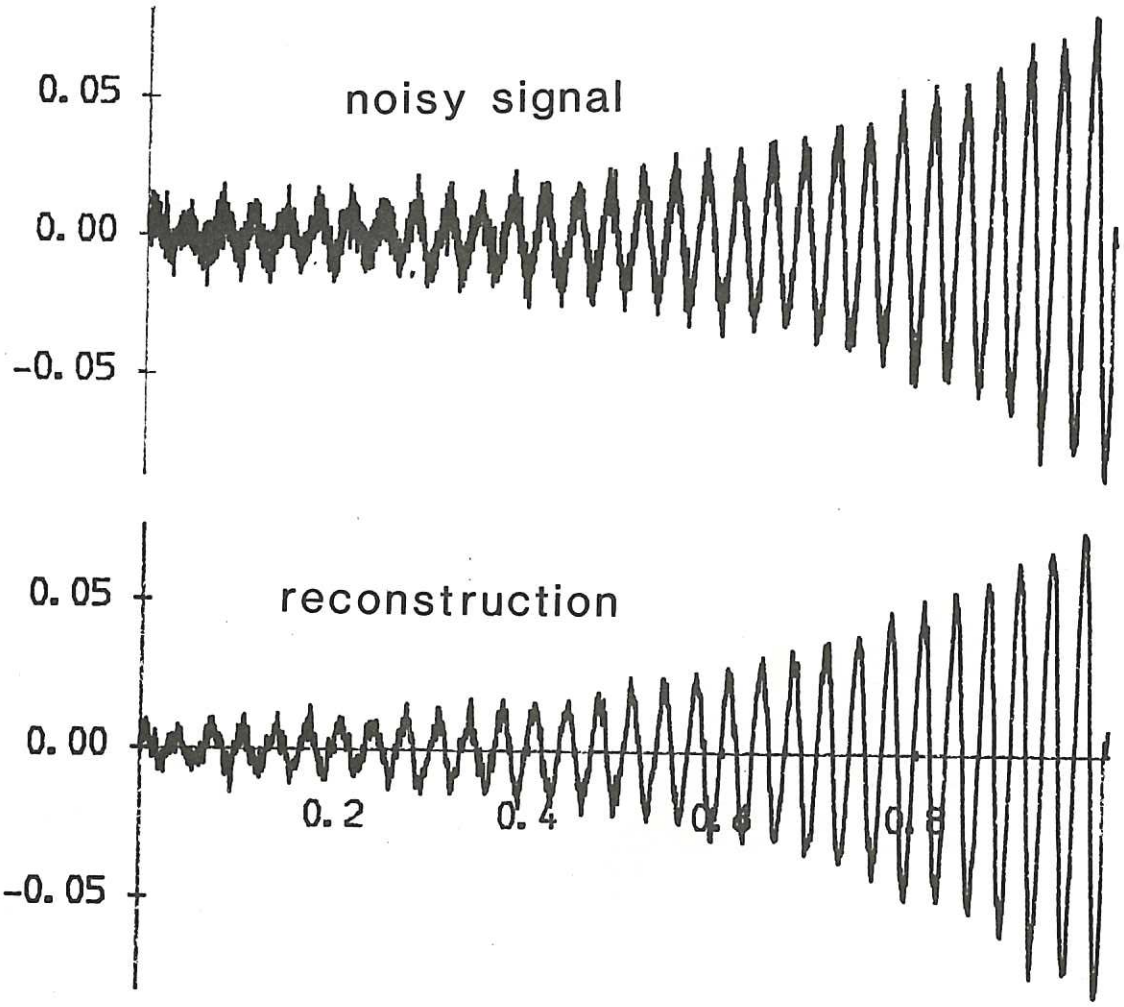

Fig. 13 The signal $f_e(t)$ with noise added as in Section 4.2 is shown top, to compare with its reconstruction (bottom) using the projections P_i corresponding to the two largest σ_i shown in Fig. 10c. The vertical scale is in arbitrary units.

CLM-R269

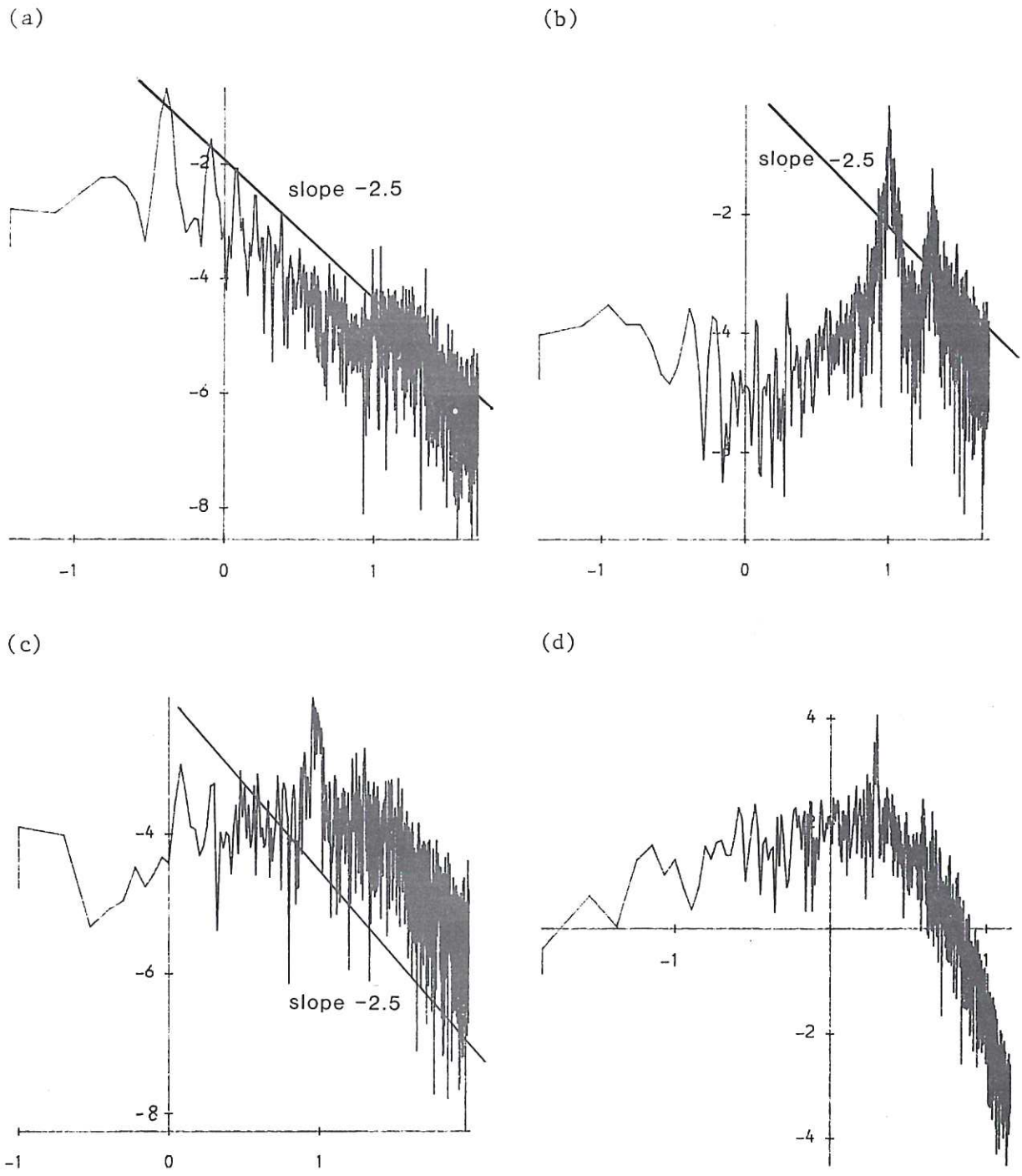

Fig. 14 Power spectra, $\log_{10} P$ plotted against $\log_{10} \omega$, where P is the power spectral density function and ω is frequency for (a) soft X-ray data and (b) Mirnov data from DITE discharge 28030, (c) Mirnov data from discharge 27649, and (d) the c-variable of the Lorenz system at the parameters listed in Section 3.3 P is in arbitrary units, while the normalisation employed for ω is such that a spike at w_s corresponds to an oscillation of duration $10^{-\omega_s}$ms (or dimensionless time units in (d)).

CLM-R269